치의과학박사 학위논문

The effect of AQP3 on intercellular adhesion in NSCLC A549 cell spheroids through cell protrusions

비소세포성 폐암 세포주 A549 spheroid에서 AQP3가 세포 돌출부를 통해 세포 간 응집에 미치는 영향

2021년 8월

서울대학교 대학원

치의과학과 종양및발달생물학 전공

민 솔

The effect of AQP3 on intercellular adhesion in NSCLC A549 cell spheroids through cell protrusions

지도교수 노 상 호

이 논문을 치의과학박사 학위논문으로 제출함
2021년 6월

서울대학교 대학원
치의과학과 종양및발달생물학 전공
민 솔

민 솔의 치의과학박사 학위논문을 인준함
2021년 7월

위 원 장 _____

부 위 원 장 _____

위 원 _____

위 원 _____

위 원 _____

Abstract

The effect of AQP3 on intercellular adhesion in NSCLC A549 cell spheroids through cell protrusions

Sol Min

Department of Cancer and Developmental Biology

The Graduate School

Seoul National University

(Directed by Prof. Sangho Roh, D.V.M., Ph.D)

Tumor cell aggregation is critical for cell survival following the loss of extracellular matrix attachment and dissemination. However, the underlying mechanotransduction of clustering

solitary tumor cells is poorly understood, especially in non-small cell lung cancers (NSCLC). Here, I examined whether cell surface protrusions played an important role in facilitating the physical contact between floating cells detached from a substrate. I employed poly-2-hydroxyethyl methacrylate-based 3D culture methods to mimic *in vivo* tumor cell cluster formation. The suprastructural analysis of human NSCLC A549 cell spheroids showed that finger-like protrusions clung together via the actin cytoskeleton. Time-lapse holotomography demonstrated that the finger-like protrusions of free-floating cells in 3D culture displayed exploratory coalescence. Global gene expression analysis demonstrated that the genes in the organic hydroxyl transport were particularly enriched in the A549 cell spheroids. Particularly, the knockdown of the water channel aquaporin 3 gene (*AQP3*) impaired multicellular aggregate formation in 3D culture through the rearrangement of the actomyosin cytoskeleton. Moreover, the cells with reduced levels of AQP3 decreased their transmigration. Overall, these data indicate that cell detachment-upregulated *AQP3* contributes to cell surface

protrusions through actomyosin cytoskeleton remodeling, causing the aggressive aggregation of free-floating cells dependent on the property of the substratum and collective metastasis.

Keywords : AQP3, NSCLC, cell membrane protrusion, actin cytoskeleton, actomyosin cytoskeleton remodeling, aggregation, collective metastasis
Student Number : 2017-28511

Table of Contents

Figures

NSCLC A549 spheroid transfected with siRNA AQP3 (up) and quantification (down) in the Transwell.

Figure 22. Schematic diagram.

Tables

Abbreviations

AQP	Aquaporin
AQP3	Aquaporin 3
CAV1	Caveolin 1
CTC	Circulating tumor cell
ECM	Extracellular matrix
EMT	Epithelial-to-mesenchymal transition
ES	Enrichment score
FLNA	Filamin A
FLNB	Filamin B
FLNC	Filamin C
FMN2	Formin 2
FPKM	Fragments per kilobase of transcript per million-mapped reads
GAPDH	Glyceraldehyde 3-phosphate dehydrogenase

Abbreviations

MUC5B	Mucin 5B
NSCLC	Non-small cell lung cancers
PBS	Phosphate buffered saline
PCR	Polymerase chain reaction
poly-HEMA	poly-2-hydroxyethyl methacrylate
qRT-PCR	Quantitative real-time reverse transcription-polymerase chain reaction
ROCK	Rho-associated protein kinases
RPMI	Roswell Park Memorial Institute
SEM	Scanning electron microscope
TEM	Transmission electron microscope
TGF-β	Transforming growth factor-β
USH1C	Usher Syndrome 1C

Chapter 1. Review of Literature

1.1 Non-small cell lung cancer

Lung cancer is classified into two main histological types, small-cell lung cancer (SCLC) and non-small cell lung cancer (NSCLC) [1]. Approximately 85% of all lung cancers are NSCLC. NSCLC is divided into three main subtypes which are lung adenocarcinoma, squamous-cell lung carcinoma, and large-cell lung carcinoma [2].

Lung adenocarcinoma (LUAD) is the most common type of NSCLC in non-smokers with an increased incidence over the past few years [3]. LUAD commonly forms peripherally in the lungs, while SCLC and squamous-cell carcinoma (LUSC) tend to be centrally located. In the LUAD, the peripherally located mass with central fibrosis and pleural puckering is commonly formed [4]. Squamous-cell carcinoma (LUSC) is deeply associated with smoking and is more common in women than men, and accounts for about 20% of lung cancers [4]. The survival rate of LUSC is higher than LUAD [5]. Large-cell lung carcinoma (LCC) is comprised of less population of

NSCLC, accounting for about 10% [6]. LCC is usually peripherally located and bulky in appearance [7]. NSCLC is often diagnosed at an advanced stage, resulting a poor diagnosis [8,9]. Therefore, fundamental studies about the lung cancer metastatic process and research for suppressing lung cancer metastasis are required.

1.2 The importance of circulating tumor cell cluster in metastasis

Circulating tumor cell (CTC) cluster was first reported in 1954. Watanabe et,. al. has demonstrated that tumor cell cluster play an essential role in cancer metastasis compared to individual cells [10]. The importance of CTC clusters in metastasis was confirmed in melanoma-derived lung metastases and colon cancer-derived liver metastases model [11]. Metastasis partly depends on the size and concentration of CTC clusters. The studies for discovering the relationship between CTC clusters and the distant sites were reported and the studies to demonstrate the mechanism of CTC clusters' survival and metastasis advantages were attempted [10].

In order to understand the specialized microenvironment of CTC cluster, research on the physical properties should be conducted. Research on CTC has been steadily progressing since 1954, but studies to demonstrate cell-cell interaction in CTC clusters have been poorly understood.

1.3 The role of aquaporin 3 in cancers

Aquaporins (AQPs) are a family of water channel which are comprised of 13 mammalian members (AQP0 to −12). Aquaporin 3 (AQP3) belongs to the aquaglycoporin subtype, acts as a membrane channel of water and glycerol, and regulates fluid homeostasis [12].

5−year disease−free survival and 5−year overall survival rate decreased in AQP3 overexpressed hepatocellular carcinoma [13]. Tumor differentiation and metastasis are associated with AQP3 expression in colon cancer patients [14]. AQP3 expressed in 59 (70.2%) of 84 lung adenocarcinoma and was associated with tumor differentiation and clinical stage in adenocarcinoma [15]. Although the association of lung adenocarcinoma and AQP3 has been clinically reported, the role of AQP3 expression in lung adenocarcinoma remained to be elucidated [15].

AQP3 has been studied in many cancer types involved in tumor differentiation, metastasis, and tumor cell adhesion [16]. It has been reported that knockdown of AQP3 reduced the growth of NSCLC in 2D cultured condition [17,18]. Accordingly,

AQP3 may be involved in the early development of lung adenocarcinoma [15]. Interestingly, AQP3 could induce AQP-dependent cellular migration to form membrane protrusion, regulating water influx at the tip of a lamellipodium through actin cleavage [19]. However, the understanding of the role of AQP3 in forming membrane protrusions for survival from anoikis in the early pathogenesis of lung adenocarcinoma remains to be studied.

1.4 The types of protrusions affecting in cancer metastasis.

The morphological dynamics of the plasma membrane contribute to the movement of motile cells in dependence on various traction-generating mechanisms [20]. Early studies have reported the different types of protrusions such as blebs, lobopodia, and so on [21]. Most of the cell types move depending on the protrusions that are switch continuously with internal and external cues [22-24]. Such protrusion plasticity is known to play an important role in cancer cell migration and dissemination [20].

Blebs and lobopodian are actin-free structures. The hydrostatic pressure in the cytoplasm pushed out the plasma membrane, resulting in arising of blebs. Lobopodia which are large cylindrical protrusions appear to be pressure-driven [25].

Lamellipodia are thin (~200nm in height) sheet-like protrusions located at the leading edge of the plasma membrane. The formation of filopodia is associated with

lamellipodia, due to filopodia elongate (~30 μm) in front of the lamellipodia. Nevertheless, filipodia itself also can elongate without lamellipodia [26]. Lamellipodia and filopodia are branched actin filaments. They expand pushing out against the plasma membrane.

Glycocalyx which are carbohydrate-enriched layers are considered to be a potent cellular migration and invasion regulator. Recently, several studies reported that its highly hydrated fibrous meshwork influences tumor migration and invasion, especially in the complicated kinetics process of cellular adhesion [27]. Although 95% of cancer have glycocalyx, the studies about the role of glycocalyx in cancer progression are initial steps, it remained to be discovered [28].

Chapter 2. Introduction

Lung cancer is the leading cause of cancer-related death worldwide; approximately 85% of all lung cancers are non-small cell lung cancers (NSCLC) [29-32]. Despite advances in early detection and standard treatment, NSCLC is often diagnosed at an advanced stage and with a poor prognosis; the overall cure and survival rate for NSCLC remains low at 19%, particularly in locally advanced stage IIIA cancer [33]. Even after complete primary tumor resection, about 45% of the early-stage NSCLC patients develop local recurrences or distant metastases within 8 to 18 months [34]. Therefore, the treatment and prevention of NSCLC can be improved with a better understanding of the biology and the mechanisms of metastasis.

Cancer metastasis is manifested by a highly complex cascade of processes. Tumor cells start with invading from a primary site into the surrounding tissues and continuing as intravasation into the circulatory system and extravasation to a distant organ. The survived disseminated tumor cells may initiate the progressive outgrowth of secondary tumors in a

metastasis-receptive niche. However, metastasis is an inefficient process [35]. Approximately millions of cells per gram are disseminated from the primary tumors per day, but only a few become capable of transmigrating and surviving in a distant organ. One key limitation to successful metastasis is the death of the cells that occurs as they become detached from the extracellular matrix (ECM), which is known as anoikis, and from the neighboring cells, and undergo cell rounding, which is known as amorphosis [35,36].

Cancer cells have evolved multifaceted mechanisms, including the epithelial-to-mesenchymal transition (EMT), to safeguard against anoikis and amorphosis. Moreover, the recent work by several groups highlights the ability of the detached cells to form clusters or aggregates is another critical factor that can enhance the metastatic capacity of cancer cells [37-39]. Although metastasis has long been conceived of as a single-cell process, multicellular cell clusters, termed circulating tumor cell (CTC) clusters, of 2 to more than 10 cells tethered together have been directly observed in several steps of the metastasis cascade, including

the systemic circulation of the tumor cells in the bloodstream. Aceto et al. showed that the CTC clusters appeared to be derived from the oligoclonal clumps of primary tumor cells rather than the coalescence of single CTCs in the circulation [37].

CTC clusters are associated with poorer prognoses in many cancer types [40]. Indeed, in different mouse models, multicellular aggregates give rise to between 50 and 97% of the metastases. The formation of clusters induces multiple molecular properties, including the increase in stem cell-like traits, evasion from targeting by natural killer cells, and resistance to metabolic stress, among others. However, the underlying spatiotemporal mechanism by which the detached cells tether together to form aggregates is poorly understood. According to several studies, canonical cell adhesion proteins, including cadherin, are involved in cancer cell cluster formation [41,42]. In addition, plakoglobin was shown to hold CTCs together [37]. However, these studies were mostly performed under adhesive 2D and 3D conditions that could not replicate the *in vivo* tumor microenvironment that became

stiffer during the progression toward advanced cancer.

Matrigel is widely used ECM components secreted by Engelbreth-Holm Swarm mouse sarcoma cells. Matrigel support enhanced interaction of cells with ECM proteins. Since Matrigel is natural source, its properties including batch-to-batch variability and ill-defined composition could interfere with pharmacological studies [43]. Matrigel is not suitable for physical or biochemical manipulation, making it difficult to understand mechanistic studies of cellular behavior [44,45]. Here, I examined spatiotemporal cell interaction in the *in vivo* cancer pathological context by employing nonadhesive 3D poly-2-hydroxyethyl methacrylate (poly-HEMA) culture. 3D culture method using poly-HEMA hydrogel have been used for many years to mimic *in vitro* 3D cancer tissue architecture. Compared to ECM components, poly-HEMA is relatively inexpensive and reproducible, resulting in consistent results [43]. poly-HEMA hydrogel prevents cell spreading and cell attachment to the substratum due to its superhydrophilic nature. [46-48].

I aimed to study the role of the protrusion in the early

stage when cells detach from the substratum to form free-floating NSCLC A549 cell clusters [49]. Furthermore, my current study is the first to indicate that AQP3, a unique member of the water channel aquaporin (AQP) family [50], is essential for forming protrusions by acting as a key regulator of actomyosin cytoskeleton remodeling. I also discuss the implications of these findings in the context of multicellular metastasis in a hydrodynamic tumor microenvironment.

Chapter 3. Materials and Methods

3.1. Cell Culture and Reagents

The human pulmonary adenocarcinoma A549 cells (The Korean Cell Line Bank, Seoul, Korea) of a human alveolar basal epithelial carcinoma cell line were maintained in Roswell Park Memorial Institute (RPMI-1640) medium supplemented with 10% fetal bovine serum (Gibco, Grand Island, NY, USA). The cells were cultured at 37℃ under a humidified atmosphere with 95% air and 5% CO_2. Jasplakinolide and Y-27632 (Cayman Chemical, Ann Arbor, MI, USA) dissolved in dimethyl sulfoxide (Sigma-Aldrich, St. Louis, MO, USA) to reach a concentration of 1 mM. Rho activator II was obtained from Cytoskeleton Inc. (Denver, CO, USA). The cells were exposed to 30% deionized water and 5% sucrose to give an osmotic shock to induce hypotonic stress and hypertonic stress, respectively.

3.2. Imaging

Holotomographic images of the cells were taken on the 3D Cell-Explorer Fluo (Nanolive, Ecublens, Switzerland) using a low-power class I laser (0.2 mW/mm^2, λ = 520 nm), a 60 × dry objective (NA = 0.8), and a USB 3.0 CMOS Sony IMX174 sensor with a typical quantum efficiency of 70% at 545 nm, dark noise (typical) of 6.6 e^-, and a typical dynamic range of 73.7 dB. In the holotomographic image, the lateral (X and Y-axis) resolution was 200 nm, the Z-axis resolution was 400 nm, with a field of view of 90 × 90 × 30 μm, and the maximum temporal resolution was 0.5 fps 3D RI volume per second.

3.3. Time-lapse Imaging

Live cell imaging was conducted in a Top-Stage Incubator system (Okolab, Pozzuoli, Italy) at 37℃ with 5% CO2 and humidifying conditions. The cells were cultured in FluoroDish cell culture dishes (World Precision Instruments Inc., Sarasota, FL, USA) for this experiment.

3.4. Image Analysis

Image rendering and export were performed with the STEVE v.1.7.3496 software (Nanolive). The backgrounds were subtracted during post-processing, and all the slices of the post-processed image were exported to RI volumes and transformed into the 3D tiff format. The RI volumes in the tiff format can be read by the software FIJI. Three-dimensional RI volumes of all the slices were transformed into 2D RI maps using maximum intensity projection and exported to a time-lapse video file.

3.5. poly-HEMA Coating

First, 1.2 g of poly-HEMA (Sigma-Aldrich) was dissolved in 40 mL of 95% ethanol by mixing the solution overnight at 37℃. Then, 50 μL or 3.2 mL of the poly-HEMA stock solution were added to 96-well plates and 10-cm dishes, respectively, under the tissue culture hood; the plates and dishes were swirled for 10 min using a plate rotator. The plates were left to dry overnight and then washed with phosphate buffered saline (PBS) immediately before use.

3.6. RNA Sequencing

Total RNAs were isolated from different cell lines using Trizol (Invitrogen, Carlsbad, CA, USA). Total RNA quantity and quality were verified spectrophotometrically (Nano-Drop 2000 spectrometer; Thermo Scientific, Wilmington, DC, USA) and electrophoretically (Bioanalyzer 2100; Agilent Technologies, Palo Alto, CA, USA). To prepare Illumina-compatible libraries, a TruSeq RNA library preparation kit (Illumina, San Diego, CA, USA) was used according to the manufacturer' s instructions. In brief, mRNA purified from total RNA using polyA selection was chemically fragmented (50-bp fragment libraries) and converted into single-stranded cDNA using random hexamer priming. After this, the second strand was generated to create double-stranded cDNA that was ready for TruSeq library construction. Short double-stranded cDNA fragments were then connected with sequencing adapters, and suitable fragments were separated by agarose gel electrophoresis. Truseq RNA libraries were built by PCR amplification and quantified using quantitative PCR (qPCR) according to the qPCR Quantification Protocol

Guide. qPCR data were qualified using the Agilent Technologies 2100 Bioanalyzer (Agilent technologies). Libraries were sequenced (101-nt paired-end sequencing) using a HiSeq™ 2000 platform (Illumina). To estimate expression levels, the RNA-Seq reads were mapped to the human genome using TopHat (version 1.3.3) [51]. The reference genome sequence (hg19, Genome Reference Consortium GRCh37) and annotation data were downloaded from the UCSC website (http://genome.uscs.edu). The transcript counts at the gene level were calculated, and the relative transcript abundances were measured in fragments per kilobase of transcript per million mapped reads (FPKM) using Cufflinks software (version 1.2.1) [52]. FPKM is computed similarly to RPKM, except it accounts for the scenario in which only one end of a pair-end read is mapped [53]. Using this approach, the expression levels were measured for 37,396 Ref-Seq genes uniquely aligned based on RNA sequencing reads. Raw data were extracted as FPKM values across all samples, and samples with zero values across more than 50% of uniquely aligned genes were

excluded.

3.7. siRNA-Mediated Knockdown of *AQP3*

The transient knockdown of *AQP3* was performed using Lipofectamine™ RNAiMAX (ThermoFisher, Rockford, IL, USA). The cells were plated in a 6-well plate at a density of 3×10^5 cells per well and cultured overnight at 37℃. The following day, the cells were transfected with *AQP3* siRNA (sequence available in Table 1) or non-targeting control siRNA (OriGene, Rockville, MD, USA) using 7.5 μL of Lipofectamine™ RNAiMAX according to the manufacturer's instructions. The final concentration of the siRNA used per well was 25 pmol. After incubating for twenty-four h, the cells were divided into conventional 2D and poly-HEMA 3D cultures and incubated further for twenty-four h for the following experiments.

Table 1. Sequence information on the siRNAs used in this study.

Name	Sequence
siAQP3 (1)	GGA GUG AAG UCA GGU CAU AAG UU TC
siAQP3 (2)	GGA GCA GUG GGA CGU GUU UCU GU CA
siAQP3 (3)	GCA AGG GAC CAG UCG GAA GGG AU TC
siNegative	UUC UCC GAA CGU GUC ACG UTT ACG UGA CAC GUU CGG AGA ATT UGA CCU CAA CUA CAU GGU UTT AAC CAU GUA GUU GAG GUC ATT

3.8. qRT-PCR

Total RNA was extracted from the cultured cells using the PureLink^{TM} RNA Mini Kit (Invitrogen). The first-strand cDNA was synthesized using oligo-dT primers and M-MLV reverse transcriptase (Invitrogen). qRT-PCR reactions were performed in triplicates at a final volume of 20 μL containing TB Green Premix Ex Taq II (Takara, Shiga, Japan), 10 ng of cDNA, and 20 pmol of each primer. qRT-PCR was performed using a 7500 real-time PCR system (Applied Biosystems, Foster City, CA, USA) at 95℃ for 30 s, followed by 40 cycles of 95℃ for 5 s and 60℃ for 34 s. The glyceraldehyde 3-phosphate dehydrogenase gene (*GAPDH*) was used as an internal control in each reaction. Specific amplification was verified by performing a melting curve analysis (55-95℃, 0.5℃/s). The quantification of relative gene expressions was performed using the ΔΔCT method. The expression level of each gene was normalized to that of *GAPDH* in the same sample. Genes and their primers are listed in Table 2.

Table 2. Primers used in this study.

Gene	Forward sequence (5' to 3')	Reverse sequence (5' to 3')
AQP3	CCGTGACCTTTGCCATGTGC	TTGTCGGCGAAGTGCCAGAT
FMN2	GTTTCCTAGGCGAGTTCCATCC	CTTCTGGACAGCATCTGAGCGT
AXIN2	CAAACTTTCGCCAACCGTGGTTG	GGTGCAAAGACATAGCCAGAACC
MUC5B	CTGCTACGACAAGGACGGAAAC	AAGGCTGTGAGCGCACTGGATG
FLNA	CAACAAGTTCACTGTGGAGACCA	TGTAGGTGCCAGCCTCATAAGG
FLNB	CCTTCAAGGTGGCTGTCACTGA	CCCTCAACAGTTATGCCAAGCC
FLNC	ATGGTAGCTGCACCGTGGAGTA	TCCACCACATCCTTCACTGGCA
USH1C	TGTCTGCTGAGGTGGGATTGGA	CTGCGGCTACTCTTCAGCACAT
SLC5A11	CCAAACTCGTGCTGGAACTCCT	GTGAAGATGGTGCTGGCACTGT
SLC51B	ATGGTCCTCCTGGGAAGAAGCA	GCCTCATCCAAATGCAGGACTTC
CAV1	CCAAGGAGATCGACCTGGTCA	GCCGTCAAAACTGTGTGTCCCT
GAPDH	GTTCCAATATGATTCCACCC	GAAGATGGTGATGGGATTT

3.9. Western Blot Analysis

Cells were lysed with RIPA buffer (Santa Cruz Biotechnology, Santa Cruz, CA, USA) on ice for 30 min, and the lysates were centrifuged at 13,000 g at 4℃ for 15 min. The supernatants were incubated with 4 × Laemmli sample buffer (Bio-Rad, Hercules, CA, USA) at 95℃ for 5 min. The samples were then separated with SDS-PAGE gel and immunoblotted with the antibody against AQP3 (Alomone Labs Ltd, Jerusalem, Israel, 1/200), GAPDH (BioLegend, San Diego, CA, USA), or β-actin (Santa Cruz Biotechnology) or α-tubulin (Santa Cruz Biotechnology). β-actin, GAPDH, and α-tubulin were used as loading controls.

3.10. Immunocytochemistry

A549 cells were seeded on sterile glass coverslips, and immunocytochemical staining was performed. In short, the cells on coverslips were fixed with 4% paraformaldehyde for 10 min and permeabilized with 0.15% Triton-X 100 for 5 min. Then, the cells were blocked for 1 h with the blocking solution of 3% bovine serum albumin in PBS and incubated with the primary antibody against AQP3 for 2 h at room temperature. The cells were then incubated with Fluorescein-conjugated anti-rabbit IgG (Sigma-Aldrich) for 60 min at room temperature. The subcellular organization of the actin microfilaments was assessed by incubating the cells with rhodamine-conjugated phalloidin (Molecular Probes, Eugene, OR, USA) at a dilution of 1:200 to reach the final concentration of 1.5 units/mL. Next, the cells were washed with PBS, and the coverslips were mounted on a glass slide in 10% Mowiol 4-88, 1 μg/mL 4',6-diamidine-2-phenylindole dihydrochloride, and 25% glycerol in PBS with nuclei counterstained blue with 4',6-diamidine-2-phenylindole dihydrochloride (DAPI). Then, the cells were

observed under a confocal laser scanning microscope LSM800 (Zeiss, Oberkochen, Germany).

3.11. Scanning Electron Microscopy of Spheroids

The cell spheroids were collected using wide pipette tips and pooled into an Eppendorf tube. Following a PBS wash, the spheroids were incubated overnight in 2.5% glutaraldehyde (EMS, Hatfield, PA, USA), 1.25% paraformaldehyde (EMS), and 0.03% picric acid in 0.1 M sodium cacodylate buffer (pH 7.4) at 4 ℃. The spheroids were then washed in 0.1 M cacodylate and post-fixed with 1% osmium tetroxide (OsO4)/1.5% potassium ferrocyanide (KFeCN6) for 1 h. The samples were then washed 2 times in PBS, dehydrated with ethanol, exposed to critical-point drying, placed on glass coverslips, and subjected to platinum sputtering before imaging. Images were acquired at 20 kV at 1000-1500× magnification using scanning electron microscopy (JSM 630/OA, JEOL Ltd., Tokyo, Japan).

3.12. Transmission Electron Microscopy of Spheroids

The fixed spheroids that were serially dehydrated with ethanol were subsequently infiltrated by a mixture of ethanol and propylene oxide at the ratio of 2:1, 1:1, 1:2, or 0:1 for 1 h, and then by a mixture of propylene oxide and epoxy resin (Structure Probe, Inc., West Chester, PA, USA) at the ratio of 2:1, 1:1, or 1:2 for 1 h. Then, the spheroids were embedded in epoxy resin and loaded into capsules to be polymerized at 60 ℃ for 72 h. Following the staining of the semi-fine thin 1-μm sections with toluidine and sodium tetraborate, thin-sectioning at 80 nm was performed using a Leica EM UC7 ultramicrotome (Leica Microsystems, Wetzlar, Germany). The resulting sections were collected on copper grids and contrasted in 1% uranyl acetate solution in distilled water for 1 h at room temperature in the dark and lead citrate. The images were acquired using a JEM-1400 Flash TEM (JEOL Ltd.) at 120 kV.

3.13. Boyden Chamber Assay

The migration of A549 cells was examined using a 6.5 mm Transwell (Corning, Glendale, AZ). The cells were plated on the inserts and cultured at 37℃ in the upper chambers. After 20 h, the migrated cells that had crossed the inserts were fixed with 4% paraformaldehyde for 15 min and stained with 0.1% crystal violet (Sigma-Aldrich) for 10 min. The inserts were washed at least three times in PBS and the interior of the inserts was gently swabbed with a cotton swab to remove the nonmigrated cells. Then, the migrated cells counted as cells per field of view under phase-contrast microscopy.

3.14. Statistical analysis

All data were analyzed using the t-tests to compare two groups or one-way *ANOVA* with Bonferroni's *post hoc* test for multiple comparisons (≥3 groups). GraphPad Prism software (ver. 5.01) was employed for all analyses. A value of $p < 0.05$ was considered statistically significant. Data are expressed as means ± standard deviations.

Chapter 4. Results

4.1. Detachment of NSCLC A549 cells leads to protrusion formation

My initial interest was to understand the dissociation of strongly refractory tumor spheroids into single cells by trypsin/ethylenediaminetetraacetic acid. This observation led me to hypothesize that structures different from canonical cellular adherens junctions exist to form tight spheroids. I identified the underlying structure organizing the spheroids by analyzing the cell surfaces at the nanometer resolution with a transmission electron microscope (TEM). The cells were treated with 1 μM jasplakinolide which is known as an actin stabilizer. After 1 h, the medium was replaced with the fresh culture media. The treatment of jasplakinolide induced the changes in the state of actin polymerization. TEM images showed that monolayer cells grown under 2D adhesive culture displayed tight connections with canonical adherens junction-like structures (Figure 1).

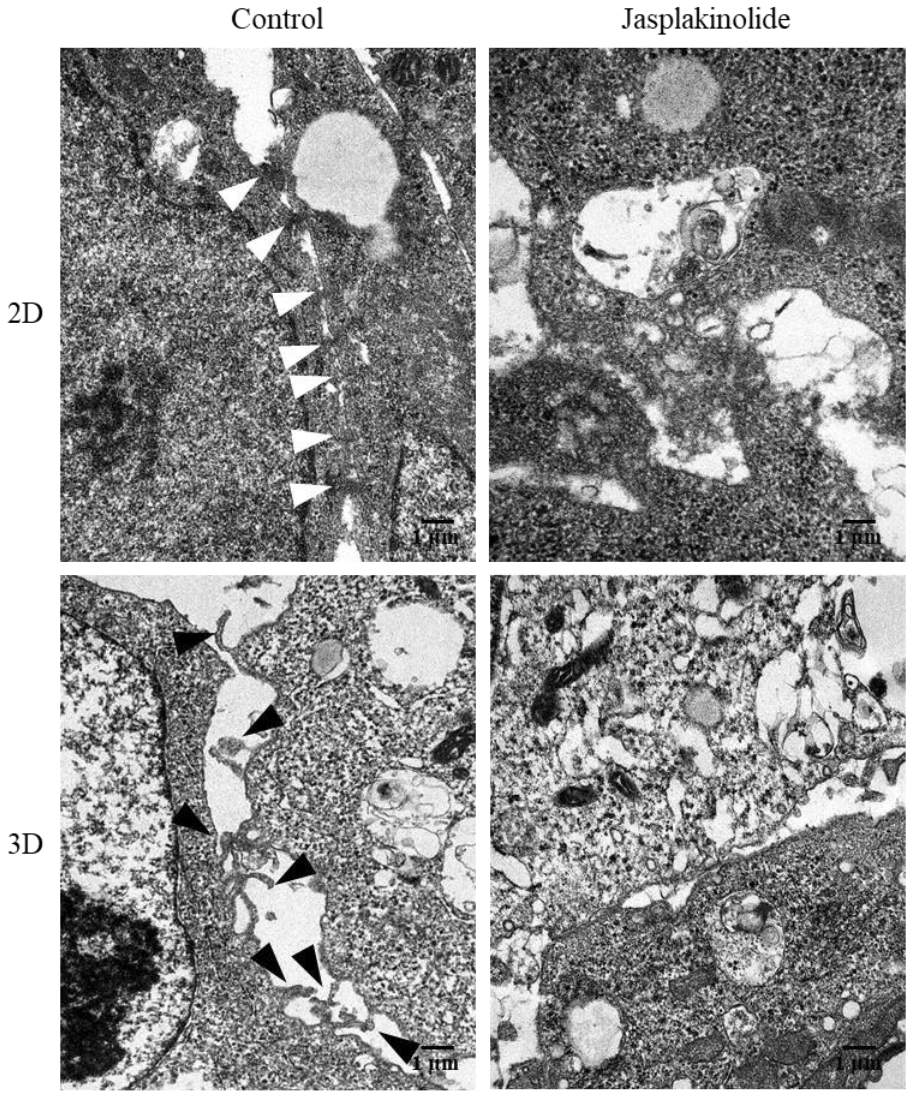

Figure 1. The representative transmission electron microscopy images of NSCLC A549 cells grown in 2D and 3D cultures. White arrowhead indicates tight junction; Black arrowhead indicates protrusion. Note the adherens junctions and protrusions. Original magnification: × 1,000. Scale bar = 200 and 100 μm.

In contrast, A549 cell spheroids exhibited protrusions from the overall cell surface but no adherens junction-like structures. Interestingly, scanning electron microscope (SEM) revealed that the changes in the state of actin cytoskeleton induced morphological changes and intercellular interaction (Figure 2). Jasplakinolide, which has been reported to activate both intrinsic and extrinsic apoptosis pathways [54], impaired the formation of A549 cell spheroids. (Figure 3). Together, these findings reveal that protrusions are critical cell surface suprastructures connecting cells in 3D tumor spheroids in a manner depending on the actin cytoskeletons.

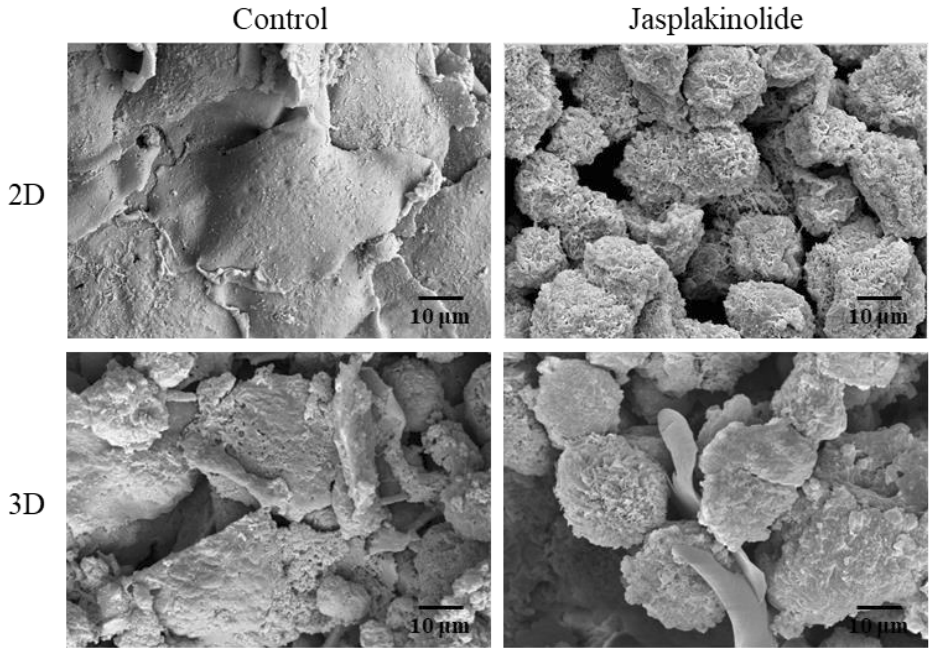

Figure 2. The representative scanning electron microscopy images of NSCLC A549 cells grown in 2D and 3D cultures.

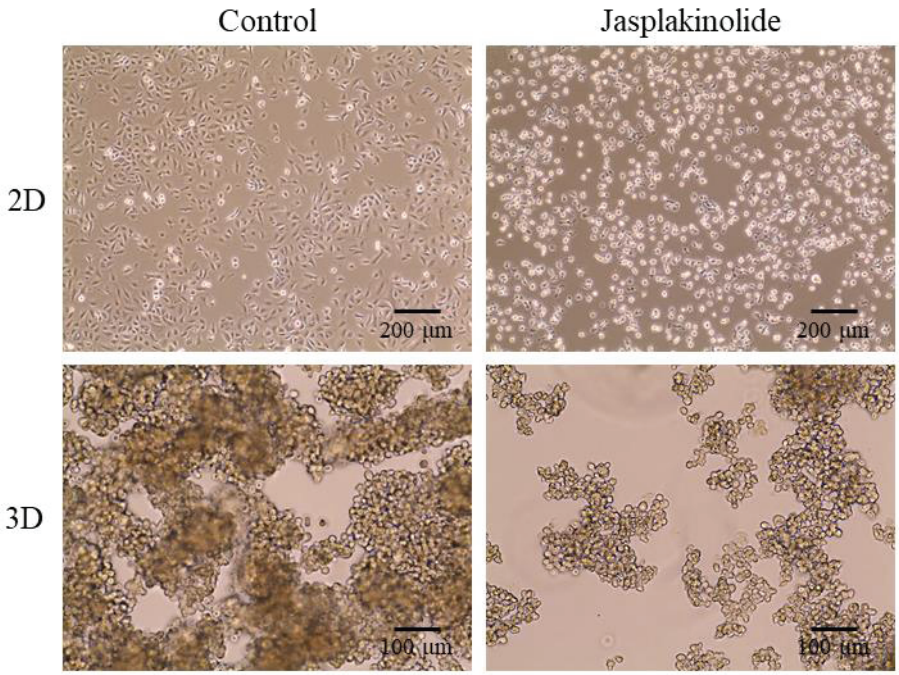

Figure 3. The phase-contrast micrographs showing the morphologies of human NSCLC A549 cells grown in 2D and 3D cultures.

4.2. Clustering of solitary human NSCLC A549 cells in an active process

The self-organizing capacity of solid tumor cells to construct 3D cellular structures was long considered a passive process: deposited on substrata where the spreading is energetically unfavorable. The cells in solution autonomously form clusters to minimize their surface energy known as surface tension, which has been related to intercellular adhesion energy [55]. A cell with lower surface tension tends to envelop one of the higher surface tension to which it adheres, result in forming cell aggregates [56]. I further examined how the protrusions interacted with each other to form the spheroids using time-lapse holotomographic microscopy, which provided information on the spatiotemporal organization of cells in 3D. The cells were analyzed upon seeding on an adhesive 2D substrate or a nonadhesive poly-HEMA 3D hydrogel. Interestingly, the detached cells occurring early upon seeding in adhesive 2D culture exhibited extension (Figure 4). Unlike the protrusions in the cell

aggregates, larger protrusions in the suspended cells on a 2D adhesive substratum are likely bleb-like structures since jasplakinolide does not change the protrusions. Larger blebs have been observed in amoeboid and lobopoid cell migration [57].

In contrast, A549 cell spheroids showed the radial sprouting of finger-like structures (Figure 4). Notably, the protrusions dynamically change their morphology, with cells moving around and repeatedly coalescing and repulsing, suggesting their importance for self-organization. It is also worth noting that the blebs disappeared after the cells attached to the substratum, whereas the finger-like protrusions in the spheroids were preserved after clustering (Figure 5). Since osmotic stress is known to affect the cytoskeleton [58], the cells were exposed to osmotic stress to identify the changes in protrusions and cell contraction. It suggested that protrusions responded dynamically to physiological changes in the hydrodynamic microenvironment. These results indicate that the finger-like protrusions in A549 cell spheroids actively cling together and form

differential spheroids in response to the diverse tumor microenvironment in relation to the osmotic and hydrostatic interstitial fluid pressures and ECM stiffness.

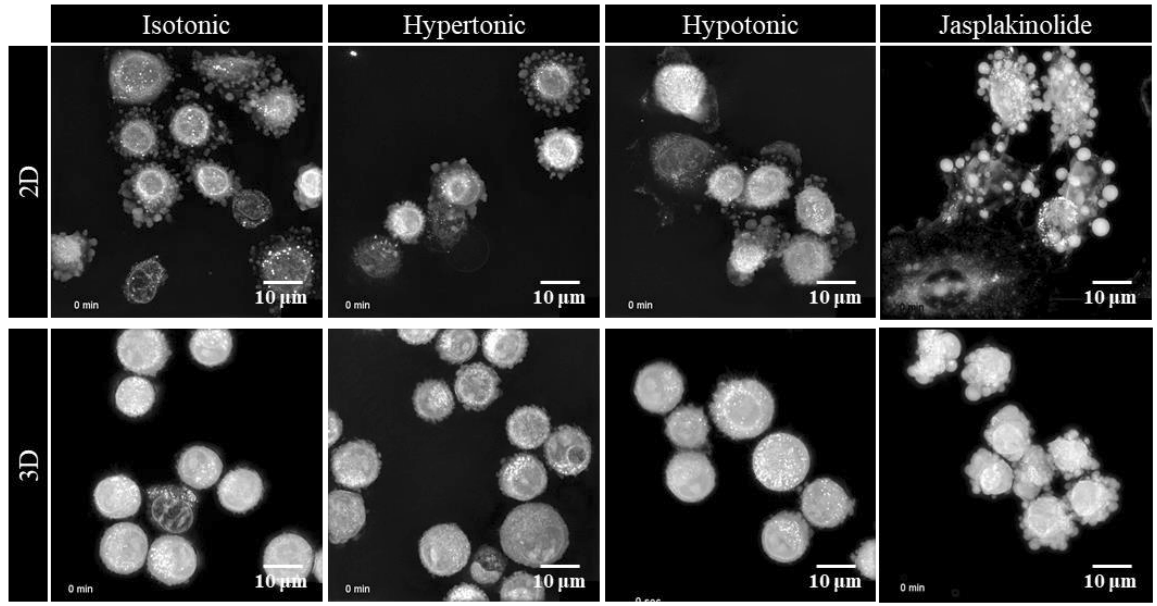

Figure 4. Representative live-cell three-dimensional holotomography of NSCLC A549 cells. The cells were exposed to 30% deionized water and 5% sucrose to give an osmotic shock to induce hypotonic stress and hypertonic stress, respectively. Images were taken for 10 h upon seeding the cells. The cells in the 3D poly-HEMA-coated nonadhesive dishes (lower panel) show exploratory protrusions compared to the cells in the 2D normal adhesive culture dish (upper panel).

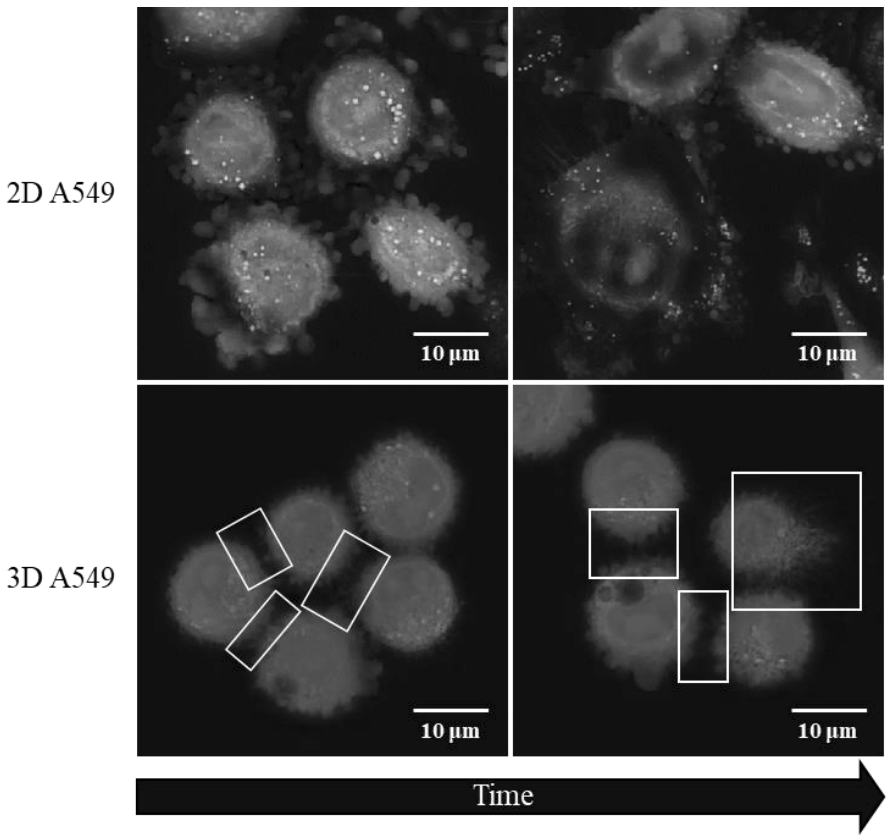

Figure 5. Time-lapse images of 2D isotonic condition. White box indicates the finger-like protrusions in 3D A549 spheroids.

4.3. Upregulation of hydrostatic pressure-regulated genes in NSCLC A549 spheroids

Several lines of evidence suggest that protrusions are dynamically controlled by the interplay of hydrostatic pressure and actomyosin cytoskeleton remodeling [59,60]. Actin-free membrane blebs are primarily controlled by hydrostatic pressure [49,61]. In contrast, finger-like protrusions accompany cofilin-mediated depolymerization and *de novo* actomyosin assembly, which requires the actin nucleators Arp2/3 complex and formin mDia1, and Rho GTPase signaling [62-64].

The expression levels (log2 fold change) of top-10 upregulated and downregulated between A549 spheroids and 2D A549 cells were investigated, reveling that *AQP3* is one of the most markedly increased genes in A549 spheroids (Figure 6, Table 3).

I further explored the underlying molecular mechanism by which A549 cells switched from extruding blebs to the actin rich finger-like protrusions depending on their substratum by

performing RNA sequencing profiling and gene set enrichment analysis (GSEA) to evaluate the global transcriptomic changes associated with protrusions. These analyses were performed with a gene set containing AQP3 which has the largest changes in its expression. The gene sets of hydroxyl transport were significantly enriched in A549 spheroids (Figure 7).

AQP3-mediated cell migration by regulating protrusion has been reported [65]. Interestingly, AQP3 transport not only water and glycerol, but hydrogen peroxide which has been reported to relate to cancer initiation and metastasis [66,67]. Given that, I hypothesize that AQP3 could play an important role in cancer initiation and metastasis by regulating protrusion in A549 spheroids.

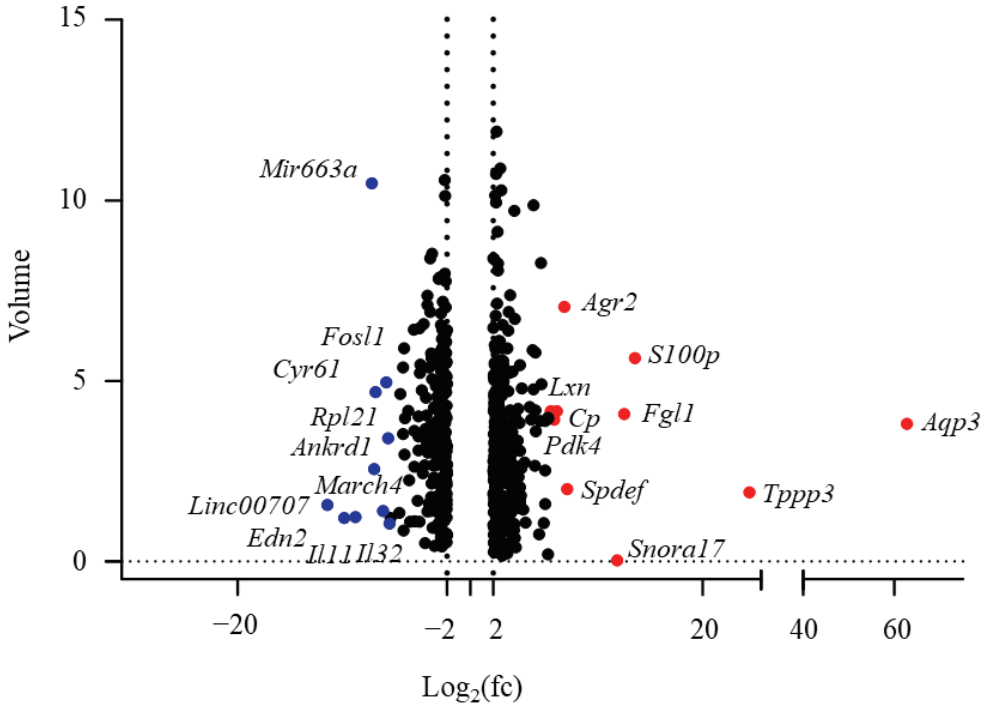

Figure 6. Volcano plot. The expression levels (log2 fold change (fc); A549 spheroid fc/A549 2D fc) of top−10 upregulated and downregulated genes.

Table 3. Fold changes in top-10 upregulated and downregulated genes.

Gene Symbol	Gene Description	[1]Fold Change (log2)
AQP3	Aquaporin 3 (Gill blood group)	62.82
TPPP3	Tubulin polymerization-promoting protein family member 3	24.03
S100P	S100 calcium binding protein P	14.16
FGL1	Fibrinogen-like 1	13.25
SNORA17	Small nucleolar RNA, H/ACA box 17	12.62
SPDEF	SAM pointed domain containing ETS transcription factor	8.35
AGR2	Anterior gradient 2	8.11
LXN	Latexin	7.43
PDK4	Pyruvate dehydrogenase kinase, isozyme 4	7.20
CP	Ceruloplasmin (ferroxidase)	6.94
MARCH4	Membrane-associated ring finger (C3HC4) 4, E3 ubiquitin protein ligase	-6.93
RPL21	Ribosomal protein L21	-7.08
FOSL1	Fos-related antigen 1 isoform 2	-7.22
LINC00707	Long intergenic non-protein coding RNA 707	-7.49
CYR61	Cysteine-rich, angiogenic inducer, 61	-8.17
ANKRD1	Ankyrin repeat domain 1 (cardiac muscle)	-8.26
MIR663A	MicroRNA 663a	-8.46
IL32	Interleukin 32	-9.88
IL11	Interleukin 11	-10.85
EDN2	Endothelin 2	-12.28

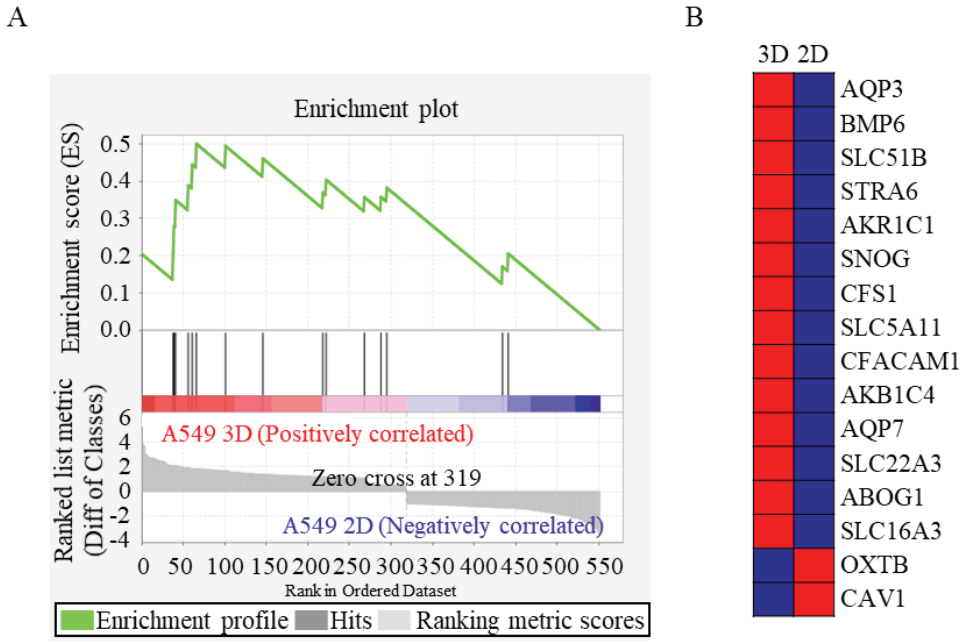

Figure 7. Global gene expression assay. (A) The enrichment plot of the gene set of organic hydroxyl transport by GSEA. Bottom panel: the plot of the ranked list of all genes, with the Y-axis indicating the value of the ranking metric and the X-axis indicating the rank for all the genes. The genes whose expression levels are most closely associated with the A549 spheroid group have the highest metric scores with positive or negative signs and are located at the left or right edge of the list. Middle panel: the location of the genes from hydroxyl transport within the ranked list. Top panel: the running enrichment score for the gene set as the analysis walks along with the ranked list. The score at the peak of the plot is the enrichment score (ES) for this gene set. The genes that appear before or at the peak are defined as core enrichment genes for this gene set. (B) The heat map of the core enrichment genes corresponding to A. The genes that contribute most to the ES, i.e., genes that appear in the ranked list before or at the peak point of ES, are defined as core enrichment genes. Rows, genes; columns, samples. The range of colors, from red to blue, indicates the range of expression values, from high to low, respectively.

The gene expression levels of signature genes for protrusion including formin 2 (*FMN2*) [68] and mucin 5b (*MUC5B*) [69] confirmed (Figure 8A). Several potential genes for protrusion were further confirmed using quantitative real-time reverse transcription-polymerase chain reaction (qPCR), suggesting gene expression levels were significantly different between 2D and 3D A549 cells (Figure 8B).

A549 spheroids exhibited elevated *AQP3* mRNA and AQP3 protein levels (Figure 8, 9). From an evaluation of each candidate gene in the GSEA and the fold change comparison, *AQP3* was of special interest. In light of the fact that genomic alteration is the underlying cause of tumor development, I conclude that *AQP3* plays a significant role in the context of tumor pathology.

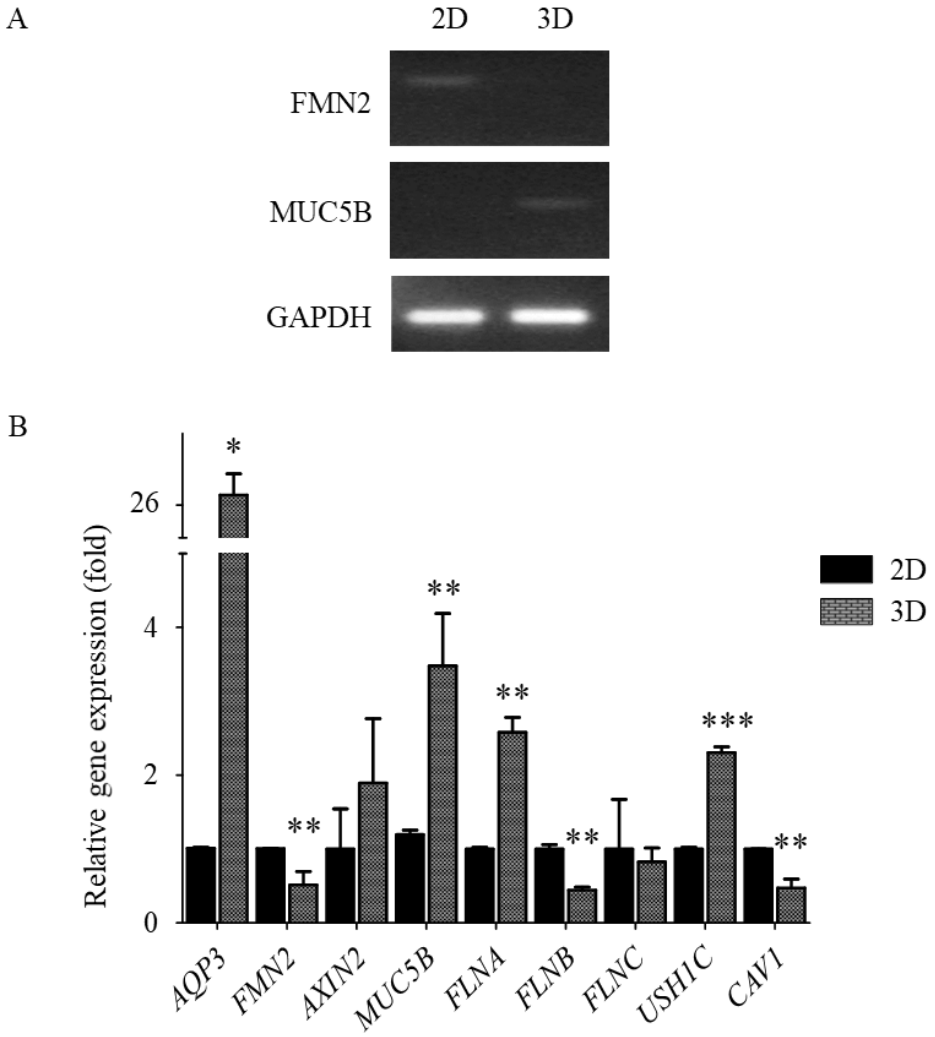

Figure 8. Gene expression levels in 2D and 3D A549 cells. (A) Polymerase chain reaction and of the transcript levels of the FMN2 and MUC5B. (B) The mRNA expression of potential genes for protrusion was measured by qPCR. The level of each mRNA was normalized against GAPDH and presented as the fold-change. The differences in expression levels were evaluated for significance using two-tailed t-tests with unequal variance. $*p < 0.05$; $** \ p < 0.01$; and $*** \ p < 0.001$.

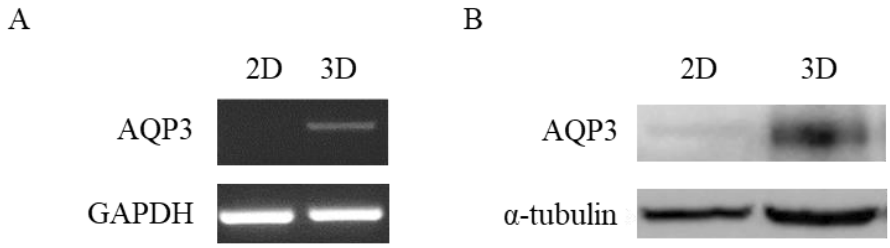

Figure 9. The expression levels of *AQP3* in 2D and 3D A549 cells. (A) Polymerase chain reaction and of the transcript levels of the *AQP3*. (B) The protein level of levels in 2D and 3D culture cells. The A549 cells were harvested following twenty-four h seeding to confirm AQP3 protein levels. α-tubulin was used as an internal control.

AQP3, in contrast to most members of the water channel aquaporin (AQP) family, can transport other small molecules, such as glycerol and H_2O_2, important for the physiological and pathological balance of hydrostatic and osmotic pressures in the plasma membrane [70]. To examine its role in the protrusion formation, LUAD A549 cells were transfected with *AQP3* siRNA to knockdown its expression. The expression of *AQP3* was found to be markedly downregulated by this siRNA, as verified by qPCR and Western blotting (Figure 10). Consistent with the expectation, I found that the knockdown of *AQP3* attenuated protrusion formation, resulting in less compact aggregates. The protrusion of 2D A549 cells was likely shift its phenotype 'bleb' to 'finger-like structure' as described in Figure 5. The numbers of blebs per cell in 2D and 3D A549 cells were counted at the early time point after seeding and decreased after transfection with *AQP3* siRNA (Figure 11).

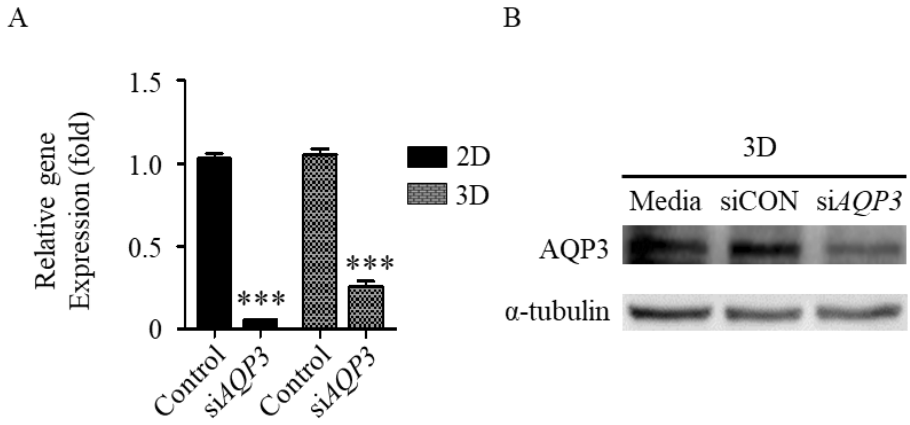

Figure 10. The expression levels of *AQP3* following *AQP3* siRNA transfection. (A) The downregulation of *AQP3* following transfection of *AQP3* siRNA. The A549 cells were pre-transfected for twenty-four h, and further incubated for twenty-four h to confirm the knockdown of *AQP3* mRNA levels. The mRNA level was normalized to that of the GAPDH mRNA in the same sample and presented as the fold-change over that of the each of control groups. The differences in expression levels were evaluated for significance using two-tailed t-tests with unequal variance. $*p < 0.05$; $** p < 0.01$; and $*** p < 0.001$. (B) The protein level of AQP3 in 3D culture cells following transfection of *AQP3* siRNA. Twenty-four h following siRNA transfection, the A549 cells were harvested to confirm the knockdown of *AQP3* by evaluating the AQP3 protein levels with Western blotting. α-tubulin was used as an internal control.

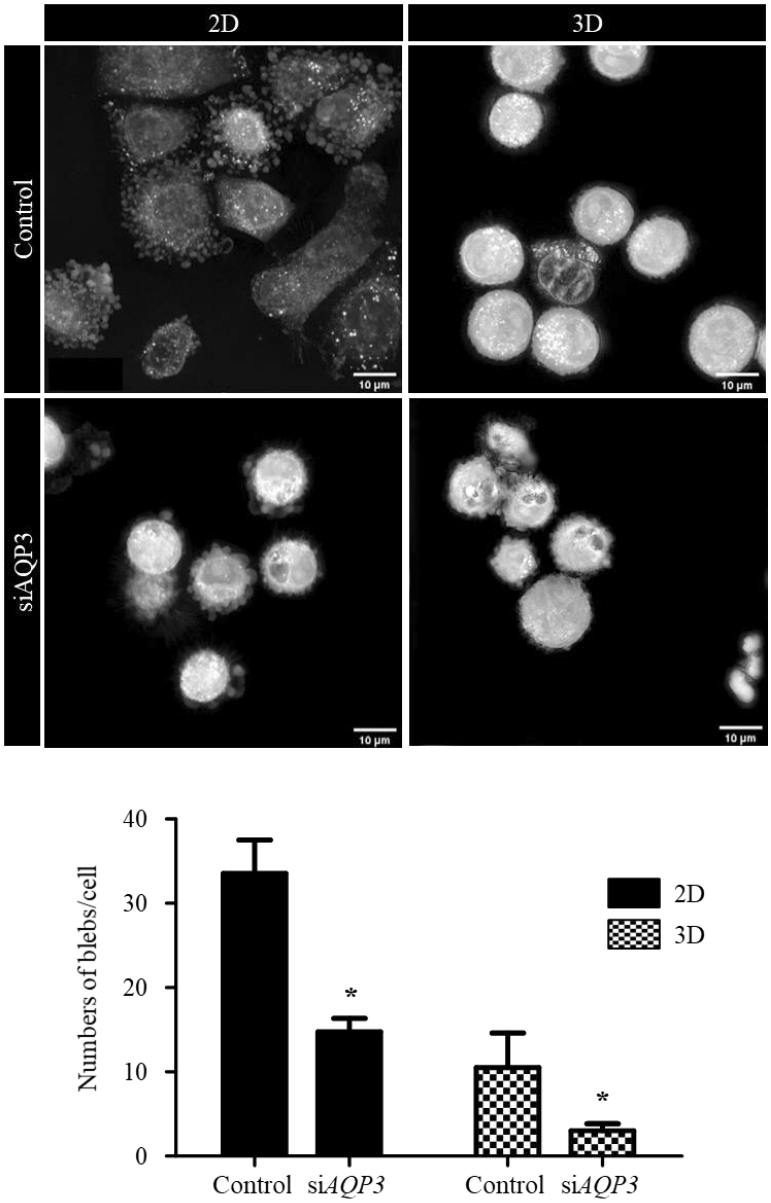

Figure 11. Live-cell three-dimensional holotomography of the A549 cells. The image shows the effect of *AQP3* knockdown on the growth behavior of the A549 cells in 2D (left) and 3D (right) cultures. Twenty-four h following siRNA transfection in the 2D culture, the cells were further incubated in the 2D or 3D culture condition.

To identify whether *AQP3* regulates aggregation, *AQP3* expression was downregulated with siRNA and monitored the phenotype and aggregation of the cells (Figure 12). The formation rate of aggregates was calculated using the ratio of non-aggregates to aggregates at the indicated time points in 3D cultured cells (Figure 13). The result indicated that the *AQP3* downregulated 3D cultured A549 cells decreased aggregation at 9 h, suggesting *AQP3* is associated with cell-cell adhesion.

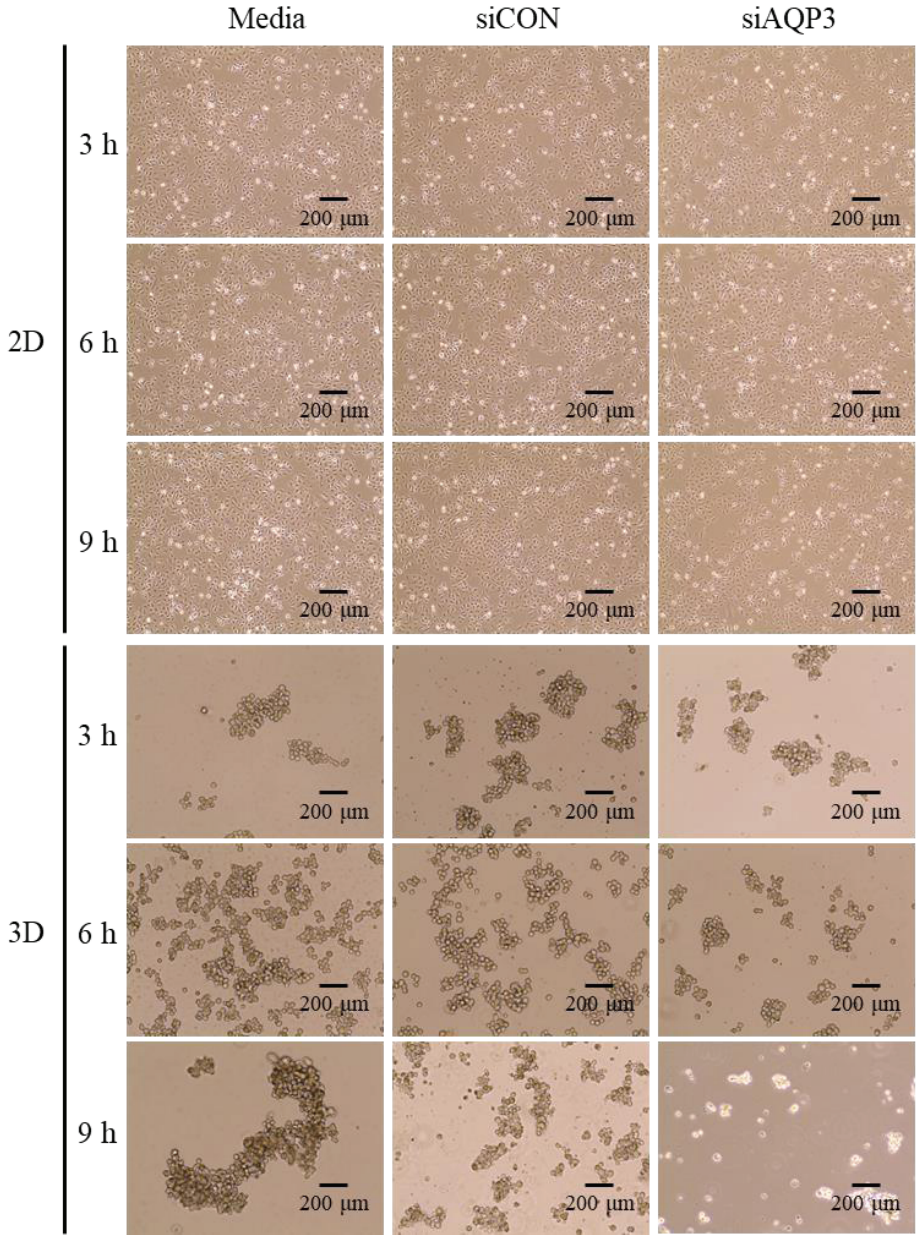

Figure 12. The phase-contrast micrograph showing the morphologies of the A549 cells grown in 2D and 3D cultures.

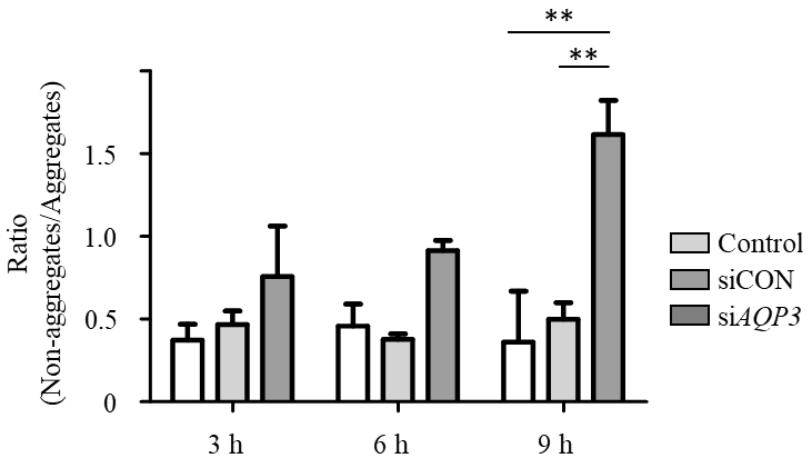

Figure 13. The ratio of non-aggregates to aggregates at the indicated time points in 3D culture condition. The differences in expression levels of *AQP3* siRNA transfected groups at each time points were evaluated for significance using two-tailed t-tests with unequal variance. $*p < 0.05$; $** \ p < 0.01$; and $*** \ p < 0.001$.

4.4. Downregulation of *AQP3* gene expression results in cortical actomyosin remodeling

Based on the result showing that A549 cells treated with actin stabilizer jasplakinolide attenuated protrusion formation (Figure 1), I hypothesized that AQP3 could control cluster formation through actomyosin in suspended culture condition. Cell rounding rearranges the cytoskeleton architecture from cell body stress fiber to cortical actomyosin, which is regulated by Rho-associated protein kinases (ROCK). In addition, cell rounding forms cortical actin in response to hydrostatic pressure induced by actomyosin contraction, resulting in the inhibition of cell shrinkage and cell death [59,60,71].

Thus, I first examined whether the protrusions in the cells under attached and suspended culture conditions were regulated by ROCK. The cells were treated with ROCK inhibitor Y-27632 and Rho activator CNF toxins (Figure 14). CNF toxins attenuated the growth of 2D A549 cells, while the combination of CNF toxins and Y-27632 recover its growth

level (Figure 14A). Unfortunately, there was the limitation in calculating 3D A549 spheroids because the cells are layered and move their position instantly as they float freely in the medium. Although cell numbers in the 3D culture condition had not been counted, the growth tendency of 3D A549 spheroids was indirectly observed by the lower magnification images (Figure 14B). The relative number of cells in each 2D group was counted and presented on the graph (Figure 15A). This result indicates that CNF toxin attenuated the spheroid growths, and the combination of CNF toxin and Y-27632 recover the growth level. Taken together, these results suggest that ROCK probably regulates the growth of A549 cell spheroids. However, there were no significant differences in AQP3 protein expression after ROCK regulator treatment, indicating that further investigations are needed to elucidate the signaling mechanism.

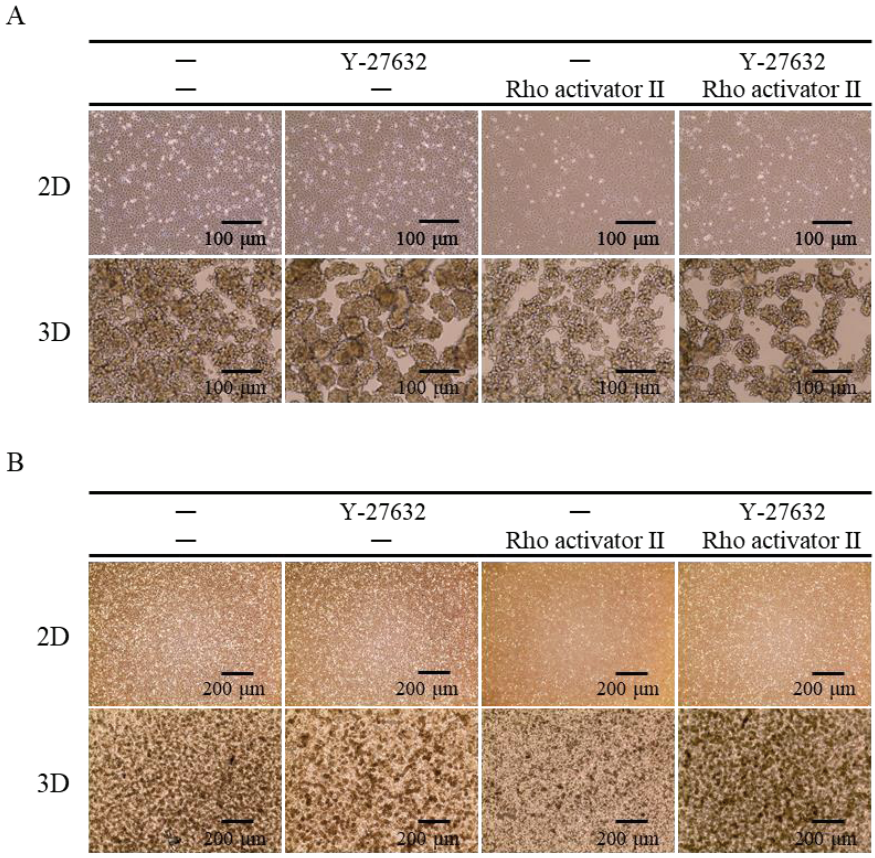

Figure 14. The effect of ROCK on A549 cell aggregation. The phase-contrast micrographs show the morphologies of the A549 cells following treatment with a ROCK inhibitor, Y-27632, and the Rho activator Ⅱ under × 100 (A) and × 40 (B).

A

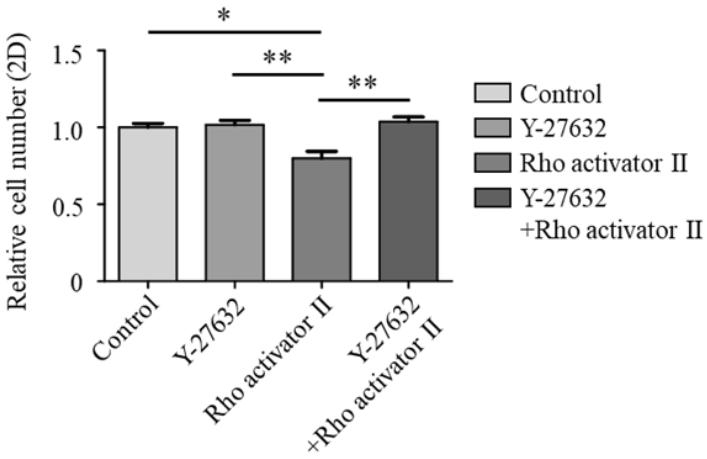

B

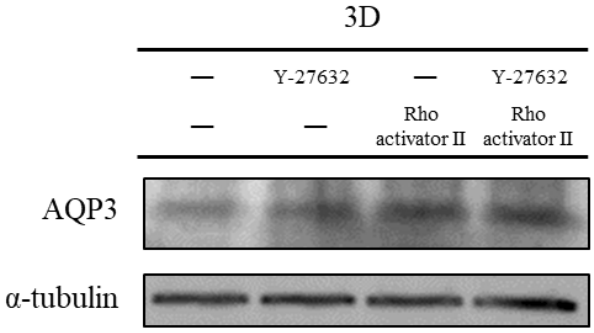

Figure 15. The effect of ROCK on A549. (A) The changes of relative cell number treated with ROCK regulators. (B) The protein level of AQP3 treated with ROCK regulators in 3D conditions.

I then investigated whether AQP3 regulated actomyosin rearrangement. The cells transfected with *AQP3* siRNA exhibited changes in cell morphology and peripheral actomyosin compared to the control siRNA-treated cells. The yellow arrowheads indicated that the morphological changes of protrusion in downregulated 2D A549 cells (Figure 16). In the 3D cell spheroids, *AQP3* siRNA tends to inhibit the formation of aggregates compared to the control siRNA-treated cells (Figure 17). At a higher magnification also showed that the cells with downregulated *AQP3* exhibited less aggregation. These data suggest that AQP3 plays a key role in protrusion formation under 3D culture conditions.

A

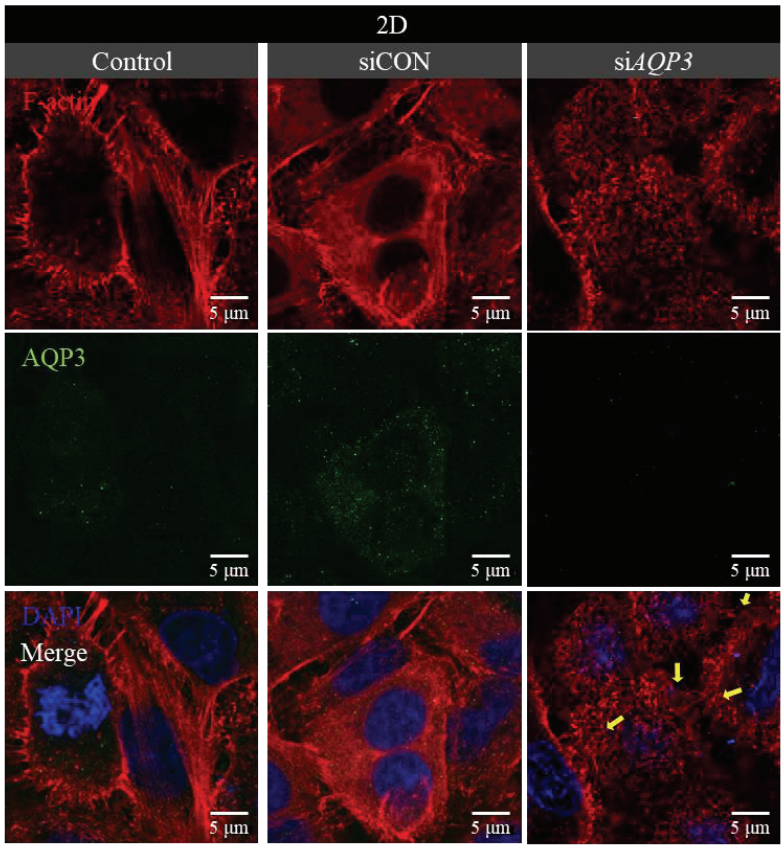

B

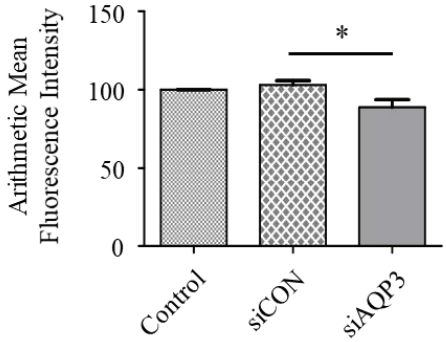

Figure 16. The effects of *AQP3* knockdown with siRNA on actomyosin cytoskeleton remodeling in 2D. (A) A549 cells were stained with anti-AQP3 antibody, followed by Fluorescein-conjugated antibody (green). The actin microfilaments were stained with rhodamine-conjugated phalloidin (red), and the nuclei were stained with DAPI (blue).

The yellow arrowheads indicate the morphological changes of protrusions. (B) The graph showed arithmetic mean fluorescence intensity of AQP3 compatible with immunofluorescence data. The differences in expression levels were evaluated for significance using one-way ANOVA followed by Tukey's post-hoc tests. * $p < 0.05$; ** $p < 0.01$; and *** $p < 0.001$.

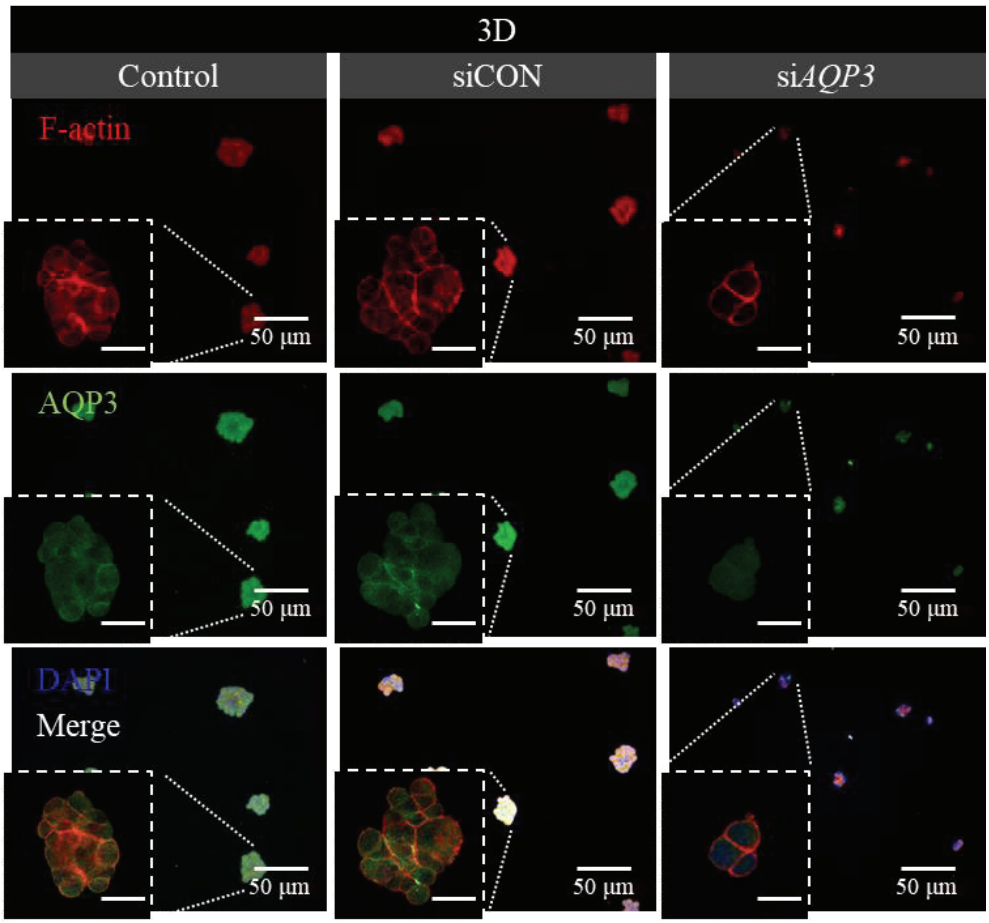

Figure 17. The effects of *AQP3* knockdown with siRNA on actomyosin cytoskeleton remodeling in 3D. A549 cells were stained with anti-AQP3 antibody, followed by Fluorescein-conjugated antibody (green). The actin microfilaments were stained with rhodamine-conjugated phalloidin (red), and the nuclei were stained with DAPI (blue). The white box indicates enlarged images of A549 spheroids of each group (scale bar = 10 μm).

ROCK activity is regulated by apoptosis [72-75]. Interestingly, A549 spheroids with downregulated *AQP3* exhibited a decreased level of anti-apoptotic marker BCL-2 along with the increase of BAX, cleaved PARP, and cleaved CASPASE 9 (Figure 18). In this study, the detailed mechanism has not been discovered, I suggest that AQP3 may regulate actomyosin cytoskeleton remodeling through the caspase pathway due to its expression was changed along with downregulation of *AQP3*.

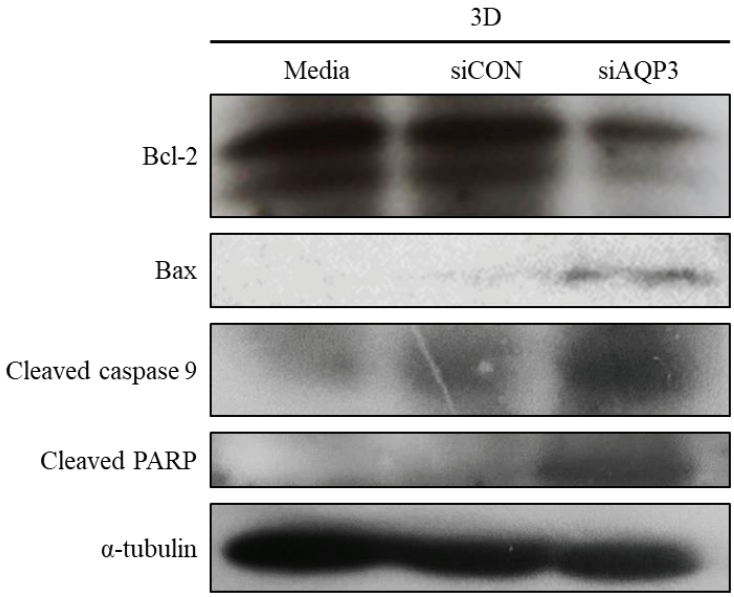

Figure 18. The effects of *AQP3* knockdown with siRNA on the apoptosis signaling pathway. Twenty-four h following siRNA transfection in 2D culture condition, the cells were further incubated in the 2D or 3D culture condition. Then, cells were harvested to confirm the effect of *AQP3* knockdown on the apoptotic molecular signatures using Western blotting. α-tubulin was used as an internal control.

I further investigated the actomyosin remodeling mechanism of AQP3 in other NSCLC cell line H460. While knockdown of *AQP3* with *AQP3* siRNA in H460 cultured in adhesive monolayer did not influence actomyosin remodeling, downregulation of *AQP3* under the 3D culture condition significantly decreased the aggregation formation and rearranged actomyosin (Figure 19). This result suggests that the actomyosin remodeling could be the underlying mechanism by which *AQP3* controls the fate of NSCLC tumor cells following substratum detachment. While the current study did not demonstrate the mechanism by which *AQP3* affected myosin II activation downstream of CASPASE 9 and PARP, it nevertheless confirmed that *AQP3* expression in cell spheroids contributed to the generation of protrusions through the apoptotic signaling pathway.

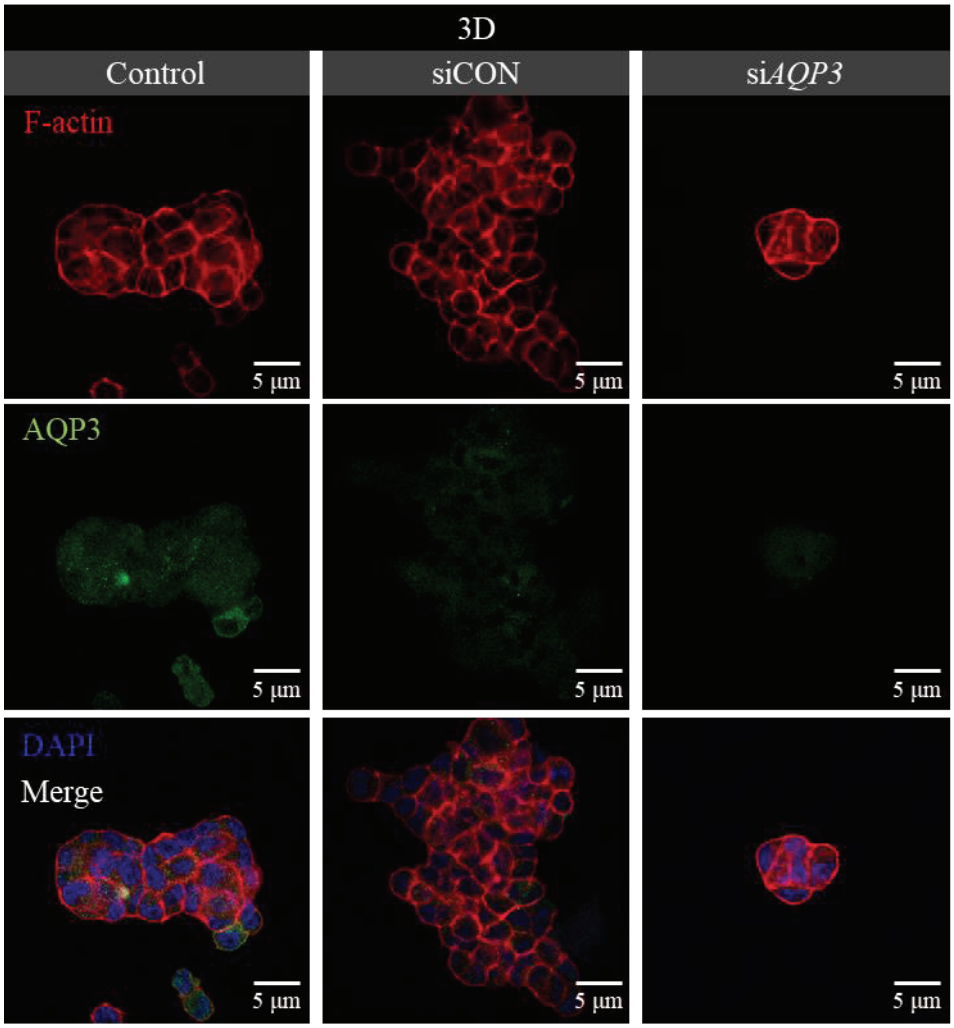

Figure 19. The effects of *AQP3* knockdown with siRNA on actomyosin cytoskeleton remodeling. H460 cells were stained with anti-AQP3 antibody, followed by Fluorescein-conjugated antibody (green). The actin microfilaments were stained with rhodamine-conjugated phalloidin (red), and the nuclei were stained with DAPI (blue).

4.5. Protrusion controls invasion in A549 cancer cells

In addition to protrusions' role in tying cells in A549 cell spheroids, I asked whether they played an important role in cell migration. Single-cell migration has been extensively studied on adhesive 2D surfaces. However, it remains unclear how aggregated cells manage to migrate for invasion and metastasis, especially in a 3D cancer environment [76-79]. Therefore, I investigated whether the protrusions of A549 spheroids could control spheroid migration.

I employed a Boyden chamber to compare the migration of the cells incubated in media. A549 cells treated with the actin stabilizer jasplakinolide decreased its migration rates on both 2D and 3D culture conditions (Figure 20). Interestingly, A549 spheroids with reduced levels of *AQP3* showed a decrease in migration (Figure 21).

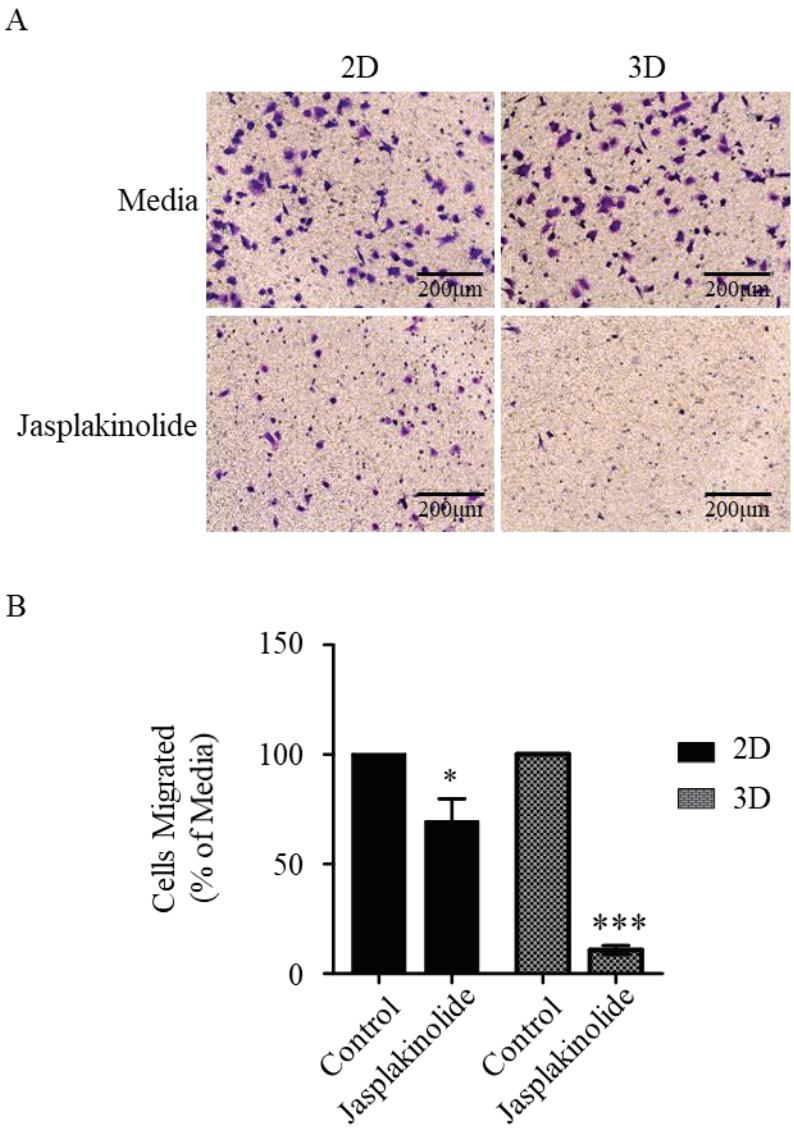

Figure 20. The phase-contrast micrograph of the migration of NSCLC A549 cells (up) and quantification (down) in the Transwell assay. The quantification of migrated cells treated with jasplakinolide represents three independent experiments, and the values represent the mean ± SEM of triplicate samples. The differences in expression levels were evaluated for significance using unpaired two-tailed t-test. * $p < 0.05$; ** $p < 0.01$; and *** $p < 0.001$.

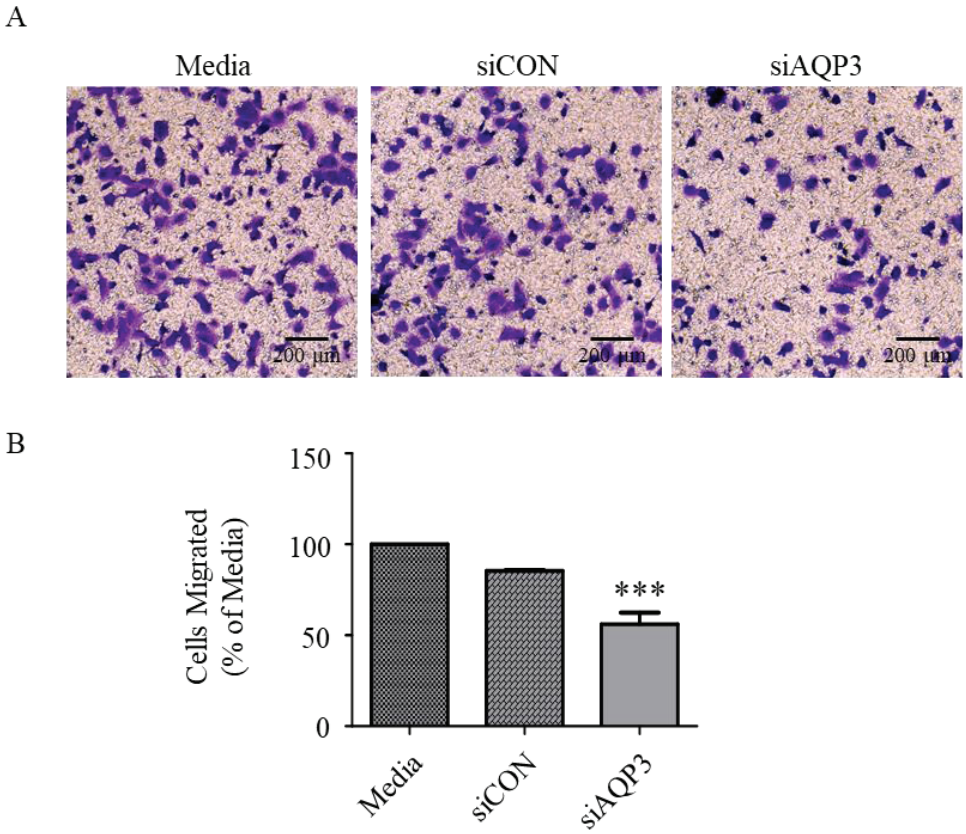

Figure 21. The phase-contrast micrograph of the migration of NSCLC A549 spheroid transfected with siRNA AQP3 (up) and quantification (down) in the Transwell. Twenty-four h following siRNA transfection in 2D culture condition, then the cells were further incubated in the 3D culture condition. The migration capacity of the A549 spheroids with a knocked down level of *AQP3* was much lower than that of the negative control cells. The differences in expression levels were evaluated for significance using one-way ANOVA followed by Tukey' s post-hoc tests. * $p < 0.05$; ** $p < 0.01$; and *** $p < 0.001$.

Chapter 5. Discussion

This study demonstrates that cell detachment-induced *AQP3* upregulation contributes to the extrusion of the cell surface to form protrusions, leading to the differential aggregation of substratum-detached cells important for multicellular metastasis in a manner dependent on the properties of the substratum.

The significance of the study is two-fold. First, there is increasing evidence showing that multicellular tumor cell aggregates are critical for cell survival following the loss of ECM attachment and dissemination through the circulatory system. The current study demonstrates that AQP3 contributes to tumor cell clustering through cell surface membrane protrusion. The AQP family comprises 13 mammalian members. While they primarily facilitate the passive transport of water across membranes, they also play a crucial role in tissue migration during embryonic development and wound healing. Furthermore, several studies have reported that this unexpected role for AQPs in cell migration is also implicated in tumor cell migration [70,80-83].

Chae and colleagues reported that AQP5 promoted tumor invasion in NSCLC. However, the mechanism underlying the AQP5-mediated invasion has not been delineated. Interestingly, the cancer genome atlas (TCGA) showed that *AQP3* in NSCLC patients undergo higher genomic alteration than other types of cancer [84]. This data suggested that *AQP3* probably play an important role in NSCLC. Indeed, my study is the first to elucidate the mechanism of AQP3 in influencing multicellular aggregation through protrusion-promoted coalescence under suspended cell growth conditions.

Second, protrusions have been extensively studied in tissue regeneration, cancer invasion and metastasis, and the environmental exploration of leukocytes [85-87]. However, many *in vitro* studies are performed with cells in adhesive flat 2D culture, under which integrin-mediated adhesion to the ECM is preserved. However, cancer invasion and metastasis occur independently of cell adhesion to ECM, as evidenced by pathological clusters isolated from patients' CTCs, ascitic fluid, and pleural effusion [46]. A study using intravital imaging reported that CTCs with active transforming growth factor-β

(TGF-β) signaling migrate as solitary cells, whereas the cells lacking TGF-β signaling invade lymphatics collectively, suggesting that TGF-β signaling regulates the mode of cancer cell motility [88]. However, the mechanisms underlying tumor aggregate formation under cancer pathological conditions remain poorly studied. Indeed, my results demonstrate for the first time that protrusions are important in 2D cellular movement and also play a critical part in the 3D aggregates of cancer cells detached from the substratum via the downstream apoptosis executor PARP and migration.

Finally, it will be interesting to elucidate the mechanism through which protrusions contribute to cell-cell adhesion in cancer clusters following substratum detachment. In this study, the term 'finger-like protrusion' was used to indicate the membrane protrusion. Under the microscope, the protrusions have similar morphologies to finger-like protrusion which has been commonly reported in the literature. Since the internal structures and components of the protrusions have not yet been studied in detail, there is a limitation to define the type of protrusion. Nevertheless, the

follow-up study in my lab has been studying protrusion. It indicated that the finger-like protrusion exhibited in my thesis has a similarity in phenotype and intercellular adhesion property to 'tube-like protrusion' which was reported by Shurer et al. [89].

Considering the studies demonstrating that hydrostatic or osmotic pressure controls cell rounding, I hypothesize that protrusion-mediated cell aggregation under suspension conditions proceeds in two steps, that protrusions should first render floating cells migratory and then adhesive. I propose that hydrostatic pressure built up locally through AQP3 channels that extrude through cell surface protrusions, acting as pedals in a fluid environment and increasing intercellular interactions to overcome Brownian dispersion. Consistent with this proposal, Saadoum et al. reported that as the underlying mechanism by which non-endothelial cells overexpressing *AQP1* or *AQP4* showed accelerated cell migration, the AQPs at the protrusions at the leading edge led to rapid water fluxes, providing the space for actomyosin assembly and flow [83]. However, it is still unclear how protrusions are adhesive and

contribute to inducing the self-assembly of the floating cells. Cell clustering in directed multicellular migration can be subdivided into cohort aggregates, in which the cells are in tight contact with each other, or streaming aggregates, in which the coordinated aggregation is not always in direct physical contact [78]. Although this study did not definitely confirm the type of aggregates in the A549 cell spheroids, it would be interesting to investigate the molecular components and viscoelastic properties of the protrusions. It would be also interesting to perform *in vivo* study to elucidate the role of protrusion in the early stage of metastasis. Addressing these ideas in detail is beyond the scope of the current study. Furthermore, my findings strongly support the idea that protrusions are a useful target in anticancer drug development, particularly targeting advanced lung cancer characterized by highly motile EMT. However, the details of the spatiotemporal architecture of the protrusions in the A549 cells and the localization of AQP3 in protrusions remain to be examined. Finally, graphical illustration of the conclusion of my study is described as below.

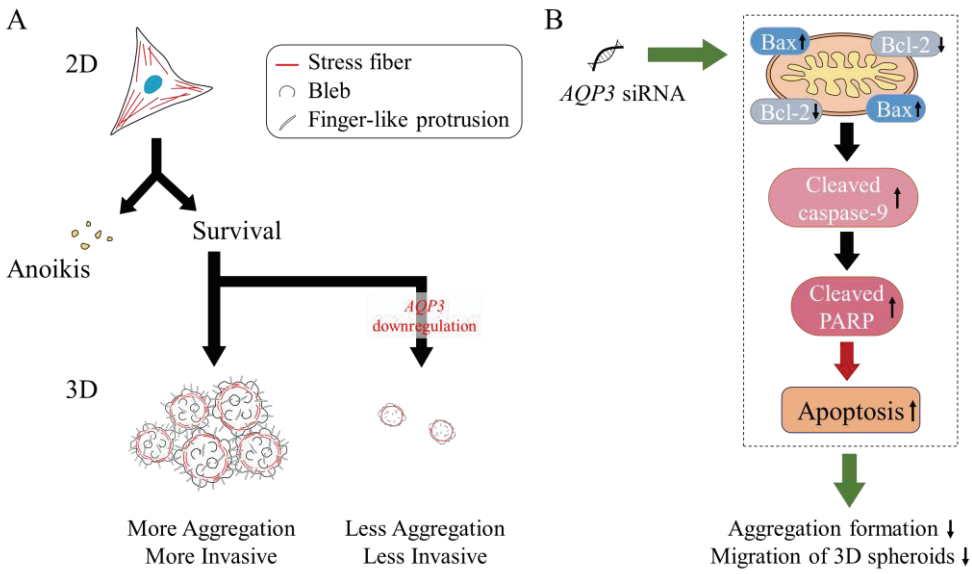

Figure 22. Schematic diagram. (A) The overall process of 3D tumor cell cluster formation. Surviving A549 cells detached from the substratum induce cluster formation by the interaction of membrane protrusions such as bleb and fingerlike protrusion. Downregulation of AQP3 reduces aggregation and migration of the cells. (B) The formation and migration of 3D spheroid of A549 cells are through the apoptosis pathway regulation by AQP3.

References

1. Molina, J.R.; Yang, P.; Cassivi, S.D.; Schild, S.E.; Adjei, A.A. Non-small cell lung cancer: epidemiology, risk factors, treatment, and survivorship. *Mayo Clin Proc* 2008, *83*, 584-594, doi:10.4065/83.5.584.
2. Inamura, K. Lung Cancer: Understanding Its Molecular Pathology and the 2015 WHO Classification. *Front Oncol* 2017, *7*, 193, doi:10.3389/fonc.2017.00193.
3. Chen, Y.J.; Roumeliotis, T.I.; Chang, Y.H.; Chen, C.T.; Han, C.L.; Lin, M.H.; Chen, H.W.; Chang, G.C.; Chang, Y.L.; Wu, C.T.; et al. Proteogenomics of Non-smoking Lung Cancer in East Asia Delineates Molecular Signatures of Pathogenesis and Progression. *Cell* 2020, *182*, 226-244 e217, doi:10.1016/j.cell.2020.06.012.
4. Zheng, M. Classification and Pathology of Lung Cancer. *Surg Oncol Clin N Am* 2016, *25*, 447-468, doi:10.1016/j.soc.2016.02.003.
5. Yang, Z.; Peng, Y.; Guo, W.; Xu, J.; Li, L.; Tian, H.; Li, R.; Liu, L.; Tan, F.; Gao, S.; et al. PD-L1 and CD47 co-expression predicts survival and enlightens future dual-targeting immunotherapy in non-small cell lung cancer. *Thorac Cancer* 2021, *12*, 1743-1751, doi:10.1111/1759-7714.13989.
6. Xiaochuan, L.; Jiangyong, Y.; Ping, Z.; Xiaonan, W.; Lin, L. Clinical characteristics and prognosis of pulmonary large cell carcinoma: A population-based retrospective study using SEER data. *Thorac Cancer* 2020, *11*, 1522-1532, doi:10.1111/1759-7714.13420.
7. Purandare, N.C.; Rangarajan, V. Imaging of lung cancer: Implications on staging and management. *Indian J Radiol Imaging* 2015, *25*, 109-120, doi:10.4103/0971-3026.155831.
8. Birring, S.S.; Peake, M.D. Symptoms and the early diagnosis of lung cancer. *Thorax* 2005, *60*, 268-269, doi:10.1136/thx.2004.032698.
9. Blandin Knight, S.; Crosbie, P.A.; Balata, H.; Chudziak, J.; Hussell, T.; Dive, C. Progress and prospects of early detection in lung cancer. *Open Biol* 2017, *7*, doi:10.1098/rsob.170070.
10. Watanabe, S. The metastasizability of tumor cells. *Cancer* 1954, *7*, 215-223, doi:10.1002/1097-0142(195403)7:2<215::aid-cncr2820070203>3.0.co;2-6.
11. Hong, Y.; Fang, F.; Zhang, Q. Circulating tumor cell clusters: What we know and what we expect (Review). *Int J Oncol* 2016, *49*, 2206-2216, doi:10.3892/ijo.2016.3747.
12. Meli, R.; Pirozzi, C.; Pelagalli, A. New Perspectives on the Potential Role of Aquaporins (AQPs) in the Physiology of Inflammation. *Front Physiol* 2018, *9*, 101, doi:10.3389/fphys.2018.00101.
13. Guo, X.; Sun, T.; Yang, M.; Li, Z.; Li, Z.; Gao, Y. Prognostic value of combined aquaporin 3 and aquaporin 5 overexpression in hepatocellular carcinoma. *Biomed Res Int* 2013, *2013*, 206525, doi:10.1155/2013/206525.

14. Li, A.; Lu, D.; Zhang, Y.; Li, J.; Fang, Y.; Li, F.; Sun, J. Critical role of aquaporin-3 in epidermal growth factor-induced migration of colorectal carcinoma cells and its clinical significance. *Oncol Rep* 2013, *29*, 535-540, doi:10.3892/or.2012.2144.
15. Liu, Y.L.; Matsuzaki, T.; Nakazawa, T.; Murata, S.; Nakamura, N.; Kondo, T.; Iwashina, M.; Mochizuki, K.; Yamane, T.; Takata, K.; et al. Expression of aquaporin 3 (AQP3) in normal and neoplastic lung tissues. *Hum Pathol* 2007, *38*, 171-178, doi:10.1016/j.humpath.2006.07.015.
16. Wang, J.; Feng, L.; Zhu, Z.; Zheng, M.; Wang, D.; Chen, Z.; Sun, H. Aquaporins as diagnostic and therapeutic targets in cancer: how far we are? *J Transl Med* 2015, *13*, 96, doi:10.1186/s12967-015-0439-7.
17. Xia, H.; Ma, Y.F.; Yu, C.H.; Li, Y.J.; Tang, J.; Li, J.B.; Zhao, Y.N.; Liu, Y. Aquaporin 3 knockdown suppresses tumour growth and angiogenesis in experimental non-small cell lung cancer. *Exp Physiol* 2014, *99*, 974-984, doi:10.1113/expphysiol.2014.078527.
18. Hou, S.Y.; Li, Y.P.; Wang, J.H.; Yang, S.L.; Wang, Y.; Wang, Y.; Kuang, Y. Aquaporin-3 Inhibition Reduces the Growth of NSCLC Cells Induced by Hypoxia. *Cell Physiol Biochem* 2016, *38*, 129-140, doi:10.1159/000438615.
19. Verkman, A.S. More than just water channels: unexpected cellular roles of aquaporins. *J Cell Sci* 2005, *118*, 3225-3232, doi:10.1242/jcs.02519.
20. Bodor, D.L.; Ponisch, W.; Endres, R.G.; Paluch, E.K. Of Cell Shapes and Motion: The Physical Basis of Animal Cell Migration. *Dev Cell* 2020, *52*, 550-562, doi:10.1016/j.devcel.2020.02.013.
21. Trinkaus, J.P. Surface activity and locomotion of Fundulus deep cells during blastula and gastrula stages. *Dev Biol* 1973, *30*, 69-103, doi:10.1016/0012-1606(73)90049-3.
22. Bergert, M.; Chandradoss, S.D.; Desai, R.A.; Paluch, E. Cell mechanics control rapid transitions between blebs and lamellipodia during migration. *Proc Natl Acad Sci U S A* 2012, *109*, 14434-14439, doi:10.1073/pnas.1207968109.
23. Te Boekhorst, V.; Preziosi, L.; Friedl, P. Plasticity of Cell Migration In Vivo and In Silico. *Annu Rev Cell Dev Biol* 2016, *32*, 491-526, doi:10.1146/annurev-cellbio-111315-125201.
24. Liu, Y.J.; Le Berre, M.; Lautenschlaeger, F.; Maiuri, P.; Callan-Jones, A.; Heuze, M.; Takaki, T.; Voituriez, R.; Piel, M. Confinement and low adhesion induce fast amoeboid migration of slow mesenchymal cells. *Cell* 2015, *160*, 659-672, doi:10.1016/j.cell.2015.01.007.
25. Petrie, R.J.; Gavara, N.; Chadwick, R.S.; Yamada, K.M. Nonpolarized signaling reveals two distinct modes of 3D cell migration. *J Cell Biol* 2012, *197*, 439-455, doi:10.1083/jcb.201201124.
26. Jacinto, A.; Wolpert, L. Filopodia. *Curr Biol* 2001, *11*, R634, doi:10.1016/s0960-9822(01)00378-5.

27. Paszek, M.J.; DuFort, C.C.; Rossier, O.; Bainer, R.; Mouw, J.K.; Godula, K.; Hudak, J.E.; Lakins, J.N.; Wijekoon, A.C.; Cassereau, L.; et al. The cancer glycocalyx mechanically primes integrin-mediated growth and survival. *Nature* 2014, *511*, 319-325, doi:10.1038/nature13535.
28. Kanyo, N.; Kovacs, K.D.; Saftics, A.; Szekacs, I.; Peter, B.; Santa-Maria, A.R.; Walter, F.R.; Der, A.; Deli, M.A.; Horvath, R. Glycocalyx regulates the strength and kinetics of cancer cell adhesion revealed by biophysical models based on high resolution label-free optical data. *Sci Rep* 2020, *10*, 22422, doi:10.1038/s41598-020-80033-6.
29. Ferlay, J.; Shin, H.R.; Bray, F.; Forman, D.; Mathers, C.; Parkin, D.M. Estimates of worldwide burden of cancer in 2008: GLOBOCAN 2008. *Int J Cancer* 2010, *127*, 2893-2917, doi:10.1002/ijc.25516.
30. Jemal, A.; Siegel, R.; Ward, E.; Hao, Y.; Xu, J.; Thun, M.J. Cancer statistics, 2009. *CA Cancer J Clin* 2009, *59*, 225-249, doi:10.3322/caac.20006.
31. Herbst, R.S.; Morgensztern, D.; Boshoff, C. The biology and management of non-small cell lung cancer. *Nature* 2018, *553*, 446-454, doi:10.1038/nature25183.
32. Herbst, R.S.; Heymach, J.V.; Lippman, S.M. Lung cancer. *N Engl J Med* 2008, *359*, 1367-1380, doi:10.1056/NEJMra0802714.
33. Walder, D.; O'Brien, M. Looking back and to the future: Are we improving 'cure' in non-small cell lung cancer? *Eur J Cancer* 2017, *75*, 192-194, doi:10.1016/j.ejca.2017.01.006.
34. Yano, T.; Okamoto, T.; Fukuyama, S.; Maehara, Y. Therapeutic strategy for postoperative recurrence in patients with non-small cell lung cancer. *World J Clin Oncol* 2014, *5*, 1048-1054, doi:10.5306/wjco.v5.i5.1048.
35. Mehlen, P.; Puisieux, A. Metastasis: a question of life or death. *Nat Rev Cancer* 2006, *6*, 449-458, doi:10.1038/nrc1886.
36. Buchheit, C.L.; Weigel, K.J.; Schafer, Z.T. Cancer cell survival during detachment from the ECM: multiple barriers to tumour progression. *Nat Rev Cancer* 2014, *14*, 632-641, doi:10.1038/nrc3789.
37. Aceto, N.; Bardia, A.; Miyamoto, D.T.; Donaldson, M.C.; Wittner, B.S.; Spencer, J.A.; Yu, M.; Pely, A.; Engstrom, A.; Zhu, H.; et al. Circulating tumor cell clusters are oligoclonal precursors of breast cancer metastasis. *Cell* 2014, *158*, 1110-1122, doi:10.1016/j.cell.2014.07.013.
38. Gkountela, S.; Castro-Giner, F.; Szczerba, B.M.; Vetter, M.; Landin, J.; Scherrer, R.; Krol, I.; Scheidmann, M.C.; Beisel, C.; Stirnimann, C.U.; et al. Circulating Tumor Cell Clustering Shapes DNA Methylation to Enable Metastasis Seeding. *Cell* 2019, *176*, 98-112 e114, doi:10.1016/j.cell.2018.11.046.
39. Labuschagne, C.F.; Cheung, E.C.; Blagih, J.; Domart, M.C.; Vousden,

K.H. Cell Clustering Promotes a Metabolic Switch that Supports Metastatic Colonization. *Cell Metab* 2019, *30*, 720–734 e725, doi:10.1016/j.cmet.2019.07.014.
40. Wrenn, E.D.; Yamamoto, A.; Moore, B.M.; Huang, Y.; McBirney, M.; Thomas, A.J.; Greenwood, E.; Rabena, Y.F.; Rahbar, H.; Partridge, S.C.; et al. Regulation of Collective Metastasis by Nanolumenal Signaling. *Cell* 2020, *183*, 395–410 e319, doi:10.1016/j.cell.2020.08.045.
41. Padmanaban, V.; Krol, I.; Suhail, Y.; Szczerba, B.M.; Aceto, N.; Bader, J.S.; Ewald, A.J. E-cadherin is required for metastasis in multiple models of breast cancer. *Nature* 2019, *573*, 439–444, doi:10.1038/s41586-019-1526-3.
42. Campbell, K.; Casanova, J. A role for E-cadherin in ensuring cohesive migration of a heterogeneous population of non-epithelial cells. *Nat Commun* 2015, *6*, 7998, doi:10.1038/ncomms8998.
43. Langhans, S.A. Three-Dimensional in Vitro Cell Culture Models in Drug Discovery and Drug Repositioning. *Front Pharmacol* 2018, *9*, 6, doi:10.3389/fphar.2018.00006.
44. Aisenbrey, E.A.; Murphy, W.L. Synthetic alternatives to Matrigel. *Nat Rev Mater* 2020, *5*, 539–551, doi:10.1038/s41578-020-0199-8.
45. Caliari, S.R.; Burdick, J.A. A practical guide to hydrogels for cell culture. *Nat Methods* 2016, *13*, 405–414, doi:10.1038/nmeth.3839.
46. Folkman, J.; Moscona, A. Role of cell shape in growth control. *Nature* 1978, *273*, 345–349, doi:10.1038/273345a0.
47. Raz, A.; Ben-Ze'ev, A. Modulation of the metastatic capability in B16 melanoma by cell shape. *Science* 1983, *221*, 1307–1310, doi:10.1126/science.6612347.
48. Choe, C.; Kim, H.; Min, S.; Park, S.; Seo, J.; Roh, S. SOX2, a stemness gene, induces progression of NSCLC A549 cells toward anchorage-independent growth and chemoresistance to vinblastine. *Onco Targets Ther* 2018, *11*, 6197–6207, doi:10.2147/OTT.S175810.
49. Krause, M.; Gautreau, A. Steering cell migration: lamellipodium dynamics and the regulation of directional persistence. *Nat Rev Mol Cell Biol* 2014, *15*, 577–590, doi:10.1038/nrm3861.
50. King, L.S.; Kozono, D.; Agre, P. From structure to disease: the evolving tale of aquaporin biology. *Nat Rev Mol Cell Biol* 2004, *5*, 687–698, doi:10.1038/nrm1469.
51. Trapnell, C.; Pachter, L.; Salzberg, S.L. TopHat: discovering splice junctions with RNA-Seq. *Bioinformatics* 2009, *25*, 1105–1111, doi:10.1093/bioinformatics/btp120.
52. Trapnell, C.; Williams, B.A.; Pertea, G.; Mortazavi, A.; Kwan, G.; van Baren, M.J.; Salzberg, S.L.; Wold, B.J.; Pachter, L. Transcript assembly and quantification by RNA-Seq reveals unannotated transcripts and isoform switching during cell differentiation. *Nat Biotechnol* 2010, *28*, 511–515, doi:10.1038/nbt.1621.

53. Lee, S.; Seo, C.H.; Lim, B.; Yang, J.O.; Oh, J.; Kim, M.; Lee, S.; Lee, B.; Kang, C.; Lee, S. Accurate quantification of transcriptome from RNA-Seq data by effective length normalization. *Nucleic Acids Res* 2011, *39*, e9, doi:10.1093/nar/gkq1015.
54. Odaka, C.; Sanders, M.L.; Crews, P. Jasplakinolide induces apoptosis in various transformed cell lines by a caspase-3-like protease-dependent pathway. *Clin Diagn Lab Immunol* 2000, *7*, 947-952, doi:10.1128/CDLI.7.6.947-952.2000.
55. Gonzalez-Rodriguez, D.; Guevorkian, K.; Douezan, S.; Brochard-Wyart, F. Soft matter models of developing tissues and tumors. *Science* 2012, *338*, 910-917, doi:10.1126/science.1226418.
56. Foty, R.A.; Steinberg, M.S. The differential adhesion hypothesis: a direct evaluation. *Dev Biol* 2005, *278*, 255-263, doi:10.1016/j.ydbio.2004.11.012.
57. Yamada, K.M.; Sixt, M. Mechanisms of 3D cell migration. *Nat Rev Mol Cell Biol* 2019, *20*, 738-752, doi:10.1038/s41580-019-0172-9.
58. Di Ciano, C.; Nie, Z.; Szaszi, K.; Lewis, A.; Uruno, T.; Zhan, X.; Rotstein, O.D.; Mak, A.; Kapus, A. Osmotic stress-induced remodeling of the cortical cytoskeleton. *Am J Physiol Cell Physiol* 2002, *283*, C850-865, doi:10.1152/ajpcell.00018.2002.
59. Coleman, M.L.; Sahai, E.A.; Yeo, M.; Bosch, M.; Dewar, A.; Olson, M.F. Membrane blebbing during apoptosis results from caspase-mediated activation of ROCK I. *Nat Cell Biol* 2001, *3*, 339-345, doi:10.1038/35070009.
60. Sebbagh, M.; Renvoize, C.; Hamelin, J.; Riche, N.; Bertoglio, J.; Breard, J. Caspase-3-mediated cleavage of ROCK I induces MLC phosphorylation and apoptotic membrane blebbing. *Nat Cell Biol* 2001, *3*, 346-352, doi:10.1038/35070019.
61. Bravo-Cordero, J.J.; Magalhaes, M.A.; Eddy, R.J.; Hodgson, L.; Condeelis, J. Functions of cofilin in cell locomotion and invasion. *Nat Rev Mol Cell Biol* 2013, *14*, 405-415, doi:10.1038/nrm3609.
62. Chugh, P.; Clark, A.G.; Smith, M.B.; Cassani, D.A.D.; Dierkes, K.; Ragab, A.; Roux, P.P.; Charras, G.; Salbreux, G.; Paluch, E.K. Actin cortex architecture regulates cell surface tension. *Nat Cell Biol* 2017, *19*, 689-697, doi:10.1038/ncb3525.
63. Ramanathan, S.P.; Helenius, J.; Stewart, M.P.; Cattin, C.J.; Hyman, A.A.; Muller, D.J. Cdk1-dependent mitotic enrichment of cortical myosin II promotes cell rounding against confinement. *Nat Cell Biol* 2015, *17*, 148-159, doi:10.1038/ncb3098.
64. Salbreux, G.; Charras, G.; Paluch, E. Actin cortex mechanics and cellular morphogenesis. *Trends Cell Biol* 2012, *22*, 536-545, doi:10.1016/j.tcb.2012.07.001.
65. Papadopoulos, M.C.; Saadoun, S. Key roles of aquaporins in tumor biology. *Biochim Biophys Acta* 2015, *1848*, 2576-2583, doi:10.1016/j.bbamem.2014.09.001.
66. Satooka, H.; Hara-Chikuma, M. Aquaporin-3 Controls Breast

Cancer Cell Migration by Regulating Hydrogen Peroxide Transport and Its Downstream Cell Signaling. *Mol Cell Biol* 2016, *36*, 1206–1218, doi:10.1128/MCB.00971-15.
67. Rodrigues, C.; Pimpao, C.; Mosca, A.F.; Coxixo, A.S.; Lopes, D.; da Silva, I.V.; Pedersen, P.A.; Antunes, F.; Soveral, G. Human Aquaporin-5 Facilitates Hydrogen Peroxide Permeation Affecting Adaption to Oxidative Stress and Cancer Cell Migration. *Cancers (Basel)* 2019, *11*, doi:10.3390/cancers11070932.
68. Isogai, T.; van der Kammen, R.; Innocenti, M. SMIFH2 has effects on Formins and p53 that perturb the cell cytoskeleton. *Sci Rep* 2015, *5*, 9802, doi:10.1038/srep09802.
69. Yuan, S.; Liu, Q.; Hu, Z.; Zhou, Z.; Wang, G.; Li, C.; Xie, W.; Meng, G.; Xiang, Y.; Wu, N.; et al. Long non-coding RNA MUC5B-AS1 promotes metastasis through mutually regulating MUC5B expression in lung adenocarcinoma. *Cell Death Dis* 2018, *9*, 450, doi:10.1038/s41419-018-0472-6.
70. Stroka, K.M.; Jiang, H.; Chen, S.H.; Tong, Z.; Wirtz, D.; Sun, S.X.; Konstantopoulos, K. Water permeation drives tumor cell migration in confined microenvironments. *Cell* 2014, *157*, 611-623, doi:10.1016/j.cell.2014.02.052.
71. Leverrier, Y.; Ridley, A.J. Apoptosis: caspases orchestrate the ROCK 'n' bleb. *Nat Cell Biol* 2001, *3*, E91-93, doi:10.1038/35070151.
72. Shi, J.; Wei, L. Rho kinase in the regulation of cell death and survival. *Arch Immunol Ther Exp (Warsz)* 2007, *55*, 61-75, doi:10.1007/s00005-007-0009-7.
73. Street, C.A.; Bryan, B.A. Rho kinase proteins--pleiotropic modulators of cell survival and apoptosis. *Anticancer Res* 2011, *31*, 3645-3657.
74. Wei, L.; Surma, M.; Shi, S.; Lambert-Cheatham, N.; Shi, J. Novel Insights into the Roles of Rho Kinase in Cancer. *Arch Immunol Ther Exp (Warsz)* 2016, *64*, 259-278, doi:10.1007/s00005-015-0382-6.
75. Okumura, N.; Fujii, K.; Kagami, T.; Makiko, N.; Kitahara, M.; Kinoshita, S.; Koizumi, N. Activation of the Rho/Rho Kinase Signaling Pathway Is Involved in Cell Death of Corneal Endothelium. *Invest Ophthalmol Vis Sci* 2016, *57*, 6843-6851, doi:10.1167/iovs.16-20123.
76. Puliafito, A.; De Simone, A.; Seano, G.; Gagliardi, P.A.; Di Blasio, L.; Chianale, F.; Gamba, A.; Primo, L.; Celani, A. Three-dimensional chemotaxis-driven aggregation of tumor cells. *Sci Rep* 2015, *5*, 15205, doi:10.1038/srep15205.
77. Roussos, E.T.; Condeelis, J.S.; Patsialou, A. Chemotaxis in cancer. *Nat Rev Cancer* 2011, *11*, 573-587, doi:10.1038/nrc3078.
78. Friedl, P.; Locker, J.; Sahai, E.; Segall, J.E. Classifying collective cancer cell invasion. *Nat Cell Biol* 2012, *14*, 777-783, doi:10.1038/ncb2548.

79. Beaune, G.; Blanch-Mercader, C.; Douezan, S.; Dumond, J.; Gonzalez-Rodriguez, D.; Cuvelier, D.; Ondarcuhu, T.; Sens, P.; Dufour, S.; Murrell, M.P.; et al. Spontaneous migration of cellular aggregates from giant keratocytes to running spheroids. *Proc Natl Acad Sci U S A* 2018, *115*, 12926-12931, doi:10.1073/pnas.1811348115.
80. Chae, Y.K.; Woo, J.; Kim, M.J.; Kang, S.K.; Kim, M.S.; Lee, J.; Lee, S.K.; Gong, G.; Kim, Y.H.; Soria, J.C.; et al. Expression of aquaporin 5 (AQP5) promotes tumor invasion in human non small cell lung cancer. *PLoS One* 2008, *3*, e2162, doi:10.1371/journal.pone.0002162.
81. Flodby, P.; Li, C.; Liu, Y.; Wang, H.; Rieger, M.E.; Minoo, P.; Crandall, E.D.; Ann, D.K.; Borok, Z.; Zhou, B. Cell-specific expression of aquaporin-5 (Aqp5) in alveolar epithelium is directed by GATA6/Sp1 via histone acetylation. *Sci Rep* 2017, *7*, 3473, doi:10.1038/s41598-017-03152-7.
82. Papadopoulos, M.C.; Saadoun, S.; Verkman, A.S. Aquaporins and cell migration. *Pflugers Arch* 2008, *456*, 693-700, doi:10.1007/s00424-007-0357-5.
83. Saadoun, S.; Papadopoulos, M.C.; Hara-Chikuma, M.; Verkman, A.S. Impairment of angiogenesis and cell migration by targeted aquaporin-1 gene disruption. *Nature* 2005, *434*, 786-792, doi:10.1038/nature03460.
84. Copy number variation (CNV) of the 28 different tumor types, GDC data portal, National cancer institute. [cited 05 July 2021], Available from:https://www.portal.gdc.cancer.gov/genes/ENSG00000165272?canDistTable_offset=10Table_offset%3D10.
85. Leithner, A.; Eichner, A.; Muller, J.; Reversat, A.; Brown, M.; Schwarz, J.; Merrin, J.; de Gorter, D.J.; Schur, F.; Bayerl, J.; et al. Diversified actin protrusions promote environmental exploration but are dispensable for locomotion of leukocytes. *Nat Cell Biol* 2016, *18*, 1253-1259, doi:10.1038/ncb3426.
86. Antonello, Z.A.; Reiff, T.; Ballesta-Illan, E.; Dominguez, M. Robust intestinal homeostasis relies on cellular plasticity in enteroblasts mediated by miR-8-Escargot switch. *EMBO J* 2015, *34*, 2025-2041, doi:10.15252/embj.201591517.
87. Morikawa, Y.; Zhang, M.; Heallen, T.; Leach, J.; Tao, G.; Xiao, Y.; Bai, Y.; Li, W.; Willerson, J.T.; Martin, J.F. Actin cytoskeletal remodeling with protrusion formation is essential for heart regeneration in Hippo-deficient mice. *Sci Signal* 2015, *8*, ra41, doi:10.1126/scisignal.2005781.
88. Giampieri, S.; Manning, C.; Hooper, S.; Jones, L.; Hill, C.S.; Sahai, E. Localized and reversible TGFbeta signalling switches breast cancer cells from cohesive to single cell motility. *Nat Cell Biol* 2009, *11*, 1287-1296, doi:10.1038/ncb1973.
89. Shurer, C.R.; Kuo, J.C.; Roberts, L.M.; Gandhi, J.G.; Colville, M.J.;

Enoki, T.A.; Pan, H.; Su, J.; Noble, J.M.; Hollander, M.J.; et al. Physical Principles of Membrane Shape Regulation by the Glycocalyx. *Cell* 2019, *177*, 1757–1770 e1721, doi:10.1016/j.cell.2019.04.017.

국문초록

비소세포성 폐암 세포주 A549 spheroid에서 AQP3가 세포 돌출부를 통해 세포 간 응집에 미치는 영향

민 솔

치의과학과

종양및발달생물학 전공

서울대학교 대학원

(지도교수: 노상호, D.V.M., Ph.D.)

종양 세포 응집은 세포 외 기질에서 분리되어 원발성 암 부위로부터 멀리 떨어진 곳으로 이동하는 전이 과정에서 세포 생존율에 중요한 영향을 미친다. 그러나 기계역학적 관점에서 고형암 세포, 특히 비소세포성 폐암(NSCLC)의 응집에 대한 연구가 드물게

보고되었다. 본 연구는 세포막 돌출물이 세포 기질에서 분리된 부유 세포 사이의 물리적 접촉을 촉진하는데 관여하는 지의 여부를 확인하였다. poly-2-hydroxyethyl methacrylate 기반 3차원 배양 방법은 생체 내 종양 세포 클러스터의 형성을 모사하기 위해 고안되었다. 인간 비소세포성 폐암 세포주 A549 spheroid의 전구조식 분석에서, 손가락 유사 돌출물 (finger-like protrusion) 구조가 액틴 세포골격을 통해 서로 밀착하였다. 타임랩스 홀로토모그래피는 3차원 배양에서, 부유 세포의 손가락 유사 돌출물 구조들이 서로 탐색하면서 유착하고자 하는 경향을 보였다. 글로벌 유전자 발현 분석 결과를 통해 organic hydroxyl transport 유전자가 A549 spheroid에 특이적으로 과발현함을 증명하였다. 특히, 물 수송 채널로 알려진 아쿠아포린 3 유전자 (AQP3)의 발현을 감소시켰을 때, 3차원 배양 환경에서 다세포 응집체의 형성을 저해하였다. 또한, AQP3가 저발현된 세포에서 트랜스마이그레이션이 감소하였다. 본 연구는 AQP3를 과발현하는 비부착 세포가 액틴 세포 골격 리모델링을 통해 세포막 돌출물 구조를 조절하고, substratum과 collective metastasis의 특성에 따라 비부착 세포의 자발적인 응집을 유발함을 확인하였다. 세포막 돌출물 구조가 암의 침습과 전이에 중요한 역할을 함이 알려졌지만 대다수의 연구가 2차원 배양 조건하에서 이루어짐을 확인하였다. 본 연구는

지지체 비의존 3차원 배양 방법을 이용하여 생체 내 종양 세포 클러스터를 모사하였고 그 결과, AQP3가 세포막 돌출물 구조를 조절하여 다세포 응집체를 이루는 세포 간 물리적 접촉에 관여함으로써 암의 진행에 영향을 미침을 밝혀내었다.

주요어: 아쿠아포린 3, 비소세포성 폐암, 세포막 돌출물, 액틴 세포 골격 리모델링, 응집, 집단 전이

학번: 2017-28511